Mechanisms for the Interannual Variability in the Tropical Indian Ocean. Part II: Regional Processes

BOHUA HUANG AND J. SHUKLA

Department of Climate Dynamics, College of Science, George Mason University, Fairfax, Virginia, and Center for Ocean–Land–Atmosphere Studies, Institute of Global Environment and Society, Calverton, Maryland

(Manuscript received 29 March 2005, in final form 12 December 2005)

ABSTRACT

To understand the mechanisms of the interannual variability in the tropical Indian Ocean, two long-term simulations are conducted using a coupled ocean–atmosphere GCM—one with active air–sea coupling over the global ocean and the other with regional coupling restricted within the Indian Ocean to the north of 30°S while the climatological monthly sea surface temperatures (SSTs) are prescribed in the uncoupled oceans to drive the atmospheric circulation. The major spatial patterns of the observed upper-ocean heat content and SST anomalies can be reproduced realistically by both simulations, suggesting that they are determined by intrinsic coupled processes within the Indian Ocean.

In both simulations, the interannual variability in the Indian Ocean is dominated by a tropical mode and a subtropical mode. The tropical mode is characterized by a coupled feedback among thermocline depth, zonal SST gradient, and wind anomalies over the equatorial and southern tropical Indian Ocean, which is strongest in boreal fall and winter. The tropical mode simulated by the global coupled model reproduces the main observational features, including a seasonal connection to the model El Niño–Southern Oscillation (ENSO). The ENSO influence, however, is weaker than that in a set of ensemble simulations described in Part I of this study, where the observed SST anomalies for 1950–98 are prescribed outside the Indian Ocean. Combining with the results from Part I of this study, it is concluded that ENSO can modulate the temporal variability of the tropical mode through atmospheric teleconnection. Its influence depends on the ENSO strength and duration. The stronger and more persistent El Niño events in the observations extend the life span of the anomalous events in the tropical Indian Ocean significantly. In the regional coupled simulation, the tropical mode is still active, but its dominant period is shifted away from that of ENSO. In the absence of ENSO forcing, the tropical mode is mainly stimulated by an anomalous atmospheric direct thermal cell forced by the fluctuations of the northwestern Pacific monsoon.

The subtropical mode is characterized by an east–west dipole pattern of the SST anomalies in the southern subtropical Indian Ocean, which is strongest in austral fall. The SST anomalies are initially forced by surface heat flux anomalies caused by the anomalous southeast trade wind in the subtropical ocean during austral summer. The trade wind anomalies are in turn associated with extratropical variations from the southern annular mode. A thermodynamic air–sea feedback strengthens these subtropical anomalies quickly in austral fall and extends their remnants into the tropical ocean in austral winter. In the simulations, this subtropical variability is independent of ENSO.

1. Introduction

This is Part II of a two-part study on the mechanisms of the interannual variability in the tropical Indian Ocean. The reader is referred to the introduction in the first part of this study (Huang and Shukla 2007, hereafter Part I) and references therein for a discussion of the motivation and background. In brief, we examine the relative importance of the regional air–sea interactions and the remote influences in producing the temporal and spatial structures of the observed interannual variability in the tropical Indian Ocean. Previous studies have emphasized the effects of the surface heat flux over the tropical Indian Ocean (e.g., Klein et al. 1999; Venzke et al. 2000; Lau and Nath 2000, 2003; Baquero-Bernal et al. 2002; Li et al. 2003; Yu and Lau 2004). In this study, we further examine the role of the ocean dynamics in the tropical air–sea feedback. We also dis-

Corresponding author address: Bohua Huang, Center for Ocean–Land–Atmosphere Studies, Institute of Global Environment and Society, 4041 Powder Mill Road #302, Calverton, MD 20705.
E-mail: huangb@cola.iges.org

DOI: 10.1175/JCLI4169.1

tinguish the tropical air–sea interaction from those in the subtropical Indian Ocean where the coupling is thermodynamic in nature (Behera and Yamagata 2001; Suzuki et al. 2004).

In Part I of this study, we examined the influences of remote forcing on the tropical Indian Ocean using the regional coupling strategy (e.g., Huang 2004) in a global ocean–atmosphere general circulation model with active air–sea coupling only within the Indian Ocean. Through an ensemble of simulations with prescribed observational sea surface temperature (SST) anomalies for 1950–98 over the oceanic region outside the tropical Indian Ocean, we have shown that the major dynamical response to the El Niño–Southern Oscillation (ENSO) forced anomalous atmospheric circulation over the Indian Basin is a pattern of opposite thermocline fluctuations between the eastern equatorial and southwestern Indian Ocean, with the former preceding the latter. This ENSO-related pattern of fluctuation explains a significant part of the Indian Ocean interannual variability during the studied period. In particular, it explains the enhanced equatorial zonal SST gradient from late boreal summer to fall and the subsequent basin-wide warming to the south of the equator in boreal winter (Huang and Shukla 2007). This set of simulations is referred to as the ensemble simulation hereafter.

A remaining question is whether this kind of basin-wide adjustment is unique to the ENSO forcing or is determined by the internal dynamics of the Indian Ocean. If the latter is true, then how is it related to the air–sea coupling within the Indian Ocean? What other internal and external factors can induce this coupled adjustment? And finally, what is the fundamental difference between the ENSO- and non-ENSO-related fluctuations? Many recent observational and model studies have demonstrated that the equatorial anomalous variations in the central and eastern Indian Ocean are at least partly independent of ENSO (e.g., Saji et al. 1999; Webster et al. 1999; Lau and Nath 2004). Yamagata et al. (2004) give a comprehensive review on these variations and their potential climate influences. However, we need to further understand the mechanisms that initiate these non-ENSO events and to find useful precursors for their prediction.

In this part of the study, we examine the coupled variability within the Indian Ocean in a model environment of suppressed Pacific ENSO. Comparing this regionally coupled model with a globally coupled simulation, we will show that, even without ENSO forcing, an interannual fluctuation of the thermocline can still be generated within the tropical Indian Ocean, which preserves the major features identified in the simulations with ENSO forcing. Therefore, the pattern of the thermocline fluctuation is intrinsic to the tropical Indian Ocean and is determined mainly by the ocean–atmosphere mean climate state and interactions within the tropical Indian Basin. In the absence of ENSO, this intrinsic pattern is stimulated by atmospheric internal fluctuations. In this paper, we will show that the leading factor that stimulates the tropical Indian Ocean mode is the atmospheric variability in the northwestern tropical Pacific. Our model study is consistent with Kajikawa et al.'s (2003) previous observational results, which found that the southeasterly wind anomalies over the southeastern Indian Ocean, a major cause of the Indian Ocean tropical variability, is triggered by the meridionally asymmetric anomalies of convections over the western Pacific between the marine continent and the South China Sea/Philippine Sea during boreal summer.

In addition to this tropically dominated mode, our model experiments show another independent mode of coupled air–sea interactions active in the southern subtropical ocean. Similar subtropical modes have been discussed previously by Behera and Yamagata (2001) using observational data and Suzuki et al. (2004) in a coupled model. Unlike the tropical mode, the subtropical SST variability is mainly associated with thermodynamic air–sea coupling. This mode is not significant in the ensemble simulation reported in Part I of this study, because it is mainly stimulated by more chaotic extratropical atmospheric fluctuations associated with the southern annular mode.

The paper is structured as follows. The model experiments are described in section 2. Section 3 examines the mean annual cycle of the model simulations in the tropical Indian Ocean as well as some relevant interannual features in the tropical Pacific and the Southern Oceans. Section 4 analyzes the interannual variability simulated by the global coupled model and with suppressed ENSO and compares them with the observations to identify the leading modes of the interannual variability in the Indian Ocean. Sections 5 and 6 further analyze the tropical and subtropical modes of variability in the Indian Ocean, respectively, to understand their physical mechanisms. A summary of the results is given in section 7.

2. Experiment design

The atmospheric and oceanic components of the coupled general circulation model (CGCM) are discussed by Schneider et al. (2001) and Schopf and Loughe (1995), respectively. These two components are referred to as the AGCM and OGCM hereafter. The AGCM is a global spectral model with a triangular

truncation of the spherical harmonics at T42, giving roughly a 2.8° latitude × 2.8° longitude resolution in the Tropics. Vertically, it is divided into 18 σ levels with higher resolution in the lower troposphere. The model has the same dynamical core as that of the National Center for Atmospheric Research Community (NCAR) Climate Model (version 3.0). Its subscale physical parameterization is state of the art, including the relaxed Arakawa–Schubert deep convection (Moorthi and Suarez 1992) and the Mellor and Yamada (1982) level 2.0 turbulent closure schemes.

The OGCM is a quasi-isopycnal model of 14 active layers. Its domain is the World Oceans within 70°S–65°N with a horizontal resolution of 1° latitude × 1.25° longitude while the meridional resolution is increased to 0.5° within 10°S–10°N. The first model layer represents the oceanic mixed layer with the entrainment at its base calculated following Niiler and Kraus (1977). The vertical mixing below the mixed layer is dependent on the Richardson number (Pacanowski and Philander 1981). The horizontal mixing is through a modified Shapiro (1970) filter. The coupling between the OGCM and the AGCM is on a daily interval. More details of the coupled system are given in Huang et al. (2004).

The model is first integrated in a globally coupled version for 500 yr. The last 300-yr simulation is analyzed in this study, which is referred to as the GLOBE run hereafter. Subsequently, the model is run in the regional coupled mode for 200 yr when the OGCM and AGCM are fully coupled in the Indian Ocean to the north of 30°S only. Outside this region, the OGCM and the AGCM are uncoupled: the monthly climatological SST derived from the fully coupled (GLOBE) run is prescribed to force the AGCM while the OGCM is forced with climatological monthly wind stress from the National Centers for Environmental Prediction (NCEP)–NCAR reanalysis (Kalnay et al. 1996). However, the OGCM still receives the AGCM-produced surface heat and freshwater fluxes on a daily interval in the uncoupled ocean, plus a relaxation term toward the same SST monthly climatology prescribed for the AGCM. Although the OGCM receives the AGCM heat fluxes in these regions, the two components remain uncoupled locally because the OGCM does not feedback to the AGCM heat fluxes there. The relaxation term is added to prevent the OGCM SST from drifting away from the prescribed CGCM climatology once the feedback is cut off. A 10°-wide zone in the South Indian Ocean within 30°–40°S blends the coupled and uncoupled portions of the domain. This regional coupling follows our previous modeling study in the tropical Atlantic Ocean (Huang et al. 2002, 2004; Huang 2004). It is similar to the settings used by Yu and Lau (2004) for an Indian Ocean study.

The simulation from the last 160 yr of this regional coupled run with climatological conditions outside the Indian Ocean is referred to as the CLIM run. The CLIM simulation is the counterpart of the ENSO-forced ensemble simulation described in Part I of this study (Huang and Shukla 2007), where the monthly observed SST anomalies for 1950–98 are superimposed on the prescribed climatological monthly SST in the uncoupled ocean to force the AGCM while real-time monthly surface wind stress and the relaxation surface heat flux force the OGCM. Opposite to the CLIM run, the ensemble simulation provides the most realistic ENSO forcing to the coupled Indian Ocean. An ensemble of multiruns from different initial conditions increases the signal-to-noise ratio of the ENSO-forced signals. Taken together, the ensemble simulation, the GLOBE run, and the CLIM run examine the Indian Ocean variability while the remote ENSO cycle is most realistic (the observed), weaker and less realistic (model produced), and totally absent. We should also point out that the CLIM experiment does not block all external influence to the Indian Ocean. The forcing can come from the atmospheric internal variability that is unrelated to air–sea feedback. An examination of this run reveals what atmospheric internal processes rejuvenate the coupled feedback processes most effectively. Since atmospheric internal variability is less periodic, it is expected that the Indian Ocean's response is closer to the intrinsic frequency of the local coupled mode.

3. Mean state and annual cycle

Before examining the interannual variability, we describe the mean state and annual cycle of the GLOBE simulation. The results from the CLIM simulation are qualitatively similar. Figure 1 shows the long-term mean temperatures from the model (left panels) and the observations (right panels), at the sea surface as well as at selected zonal and meridional cross sections for the upper ocean. The observed SST climatology is from the U.S. Climate Prediction Center (CPC) analysis (Reynolds and Smith 1994). The upper temperature climatology is from the National Oceanographic Data Center's World Ocean Database (WOD98; NODC 1999). It is clear that the model reproduces the basic structures of the observations qualitatively. Compared to the observations (Fig. 1b), the model mean SST (Fig. 1a) shows a cold bias in the equatorial and northern ocean, which is larger than 1°C to the north of 5°N and around 2°C near the northwestern coast of the Arabian Sea and some part of the Bay of Bengal. The mean SST

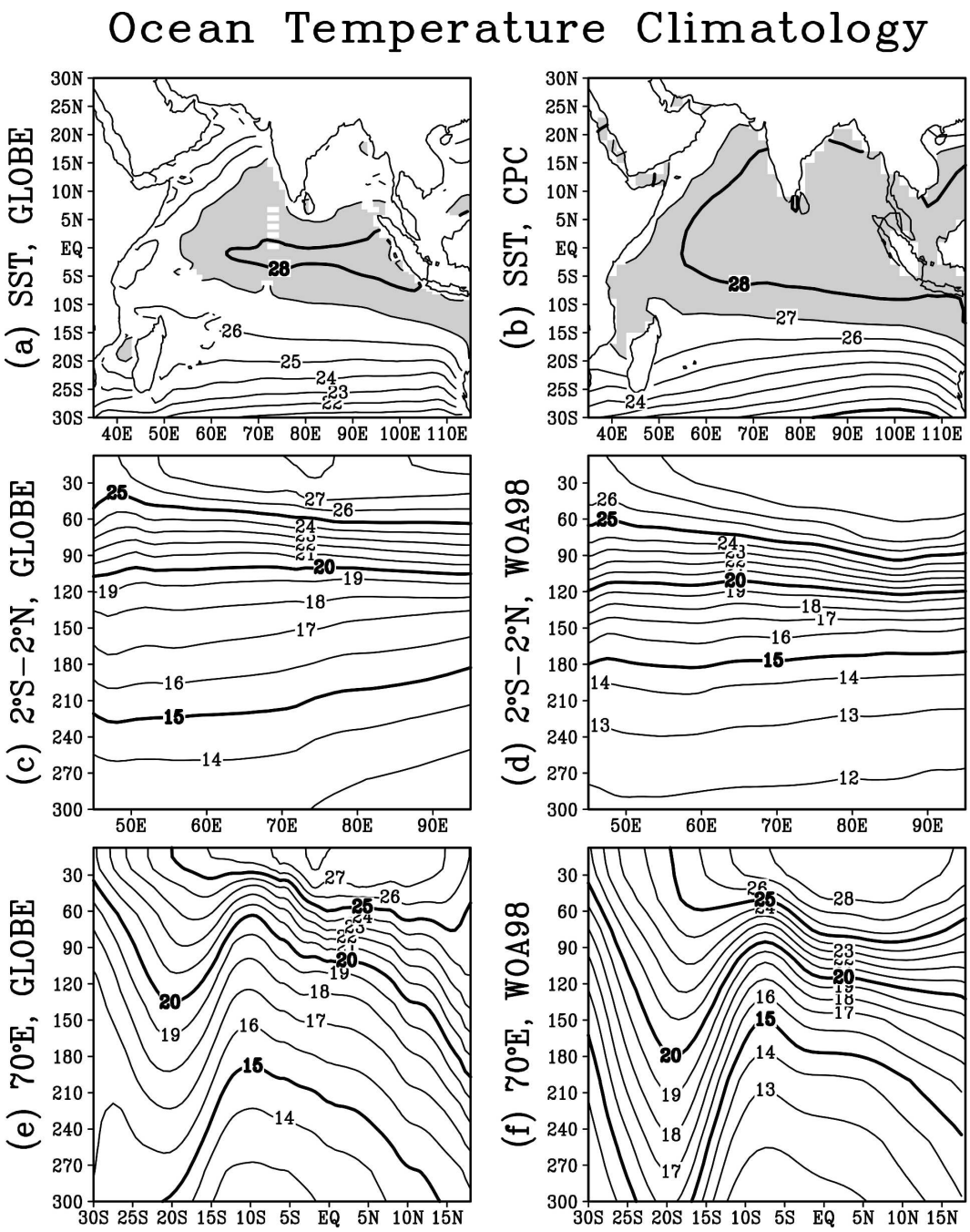

FIG. 1. The annual mean SST for (a) the GLOBE simulation and (b) the CPC analysis. Temperatures higher than 27°C are shaded. Depth–longitude sections of the ocean temperature for the upper 300 m along the equator (averaged for 2°S–2°N) for (c) the GLOBE simulation and (d) the WOD98 climatology. Depth–latitude sections of temperature along 70°E for (e) the GLOBE simulation and (f) the WOD climatology. The contour interval is 1°C for (a)–(f).

error is less than 1°C around and to the south of the equator.

Along the equator, the model 20°C isotherm is nearly flat while its 25°C isotherm deepens from west to east (Fig. 1c), which is consistent with the observations (Fig. 1d). The tilting of the upper thermocline implies weak annual mean westerlies on the equator (not shown). The model cold SST bias near the equator (around 0.8°C) is comparable to other state-of-the-art CGCMs (Davey et al. 2002). This cold bias is associated with

shallower depths of 20° and 25°C isotherms from 10 to 20 m (Figs. 1c,d). On the other hand, the model 15°C isotherm, which corresponds to the lower limit of the thermocline zone, is more than 30 m deeper than the observations in the western ocean. It reflects the fact that the model vertical temperature gradient is more diffuse in the thermocline zone than the observations. The diffusion is more seriously downward.

The model depth–latitude section at 70°E shows that a major feature of the thermocline in the southwestern Indian Ocean is the shoaling centered at 5°–10°S and a sharp deepening to its south at 20°S (Fig. 1e). Compared to the observations (Fig. 1f), the model thermocline dome is slightly biased to the south. The diffusion of the model thermocline here is similar to that along the equator. We will show in later sections that a major part of the interannual variability in the tropical Indian Ocean is associated with the low-frequency fluctuation of the thermocline depth in this region.

The monsoon circulation dominates the annual cycle in the Indian Ocean. In boreal spring [March–May (MAM, hereafter 3-month periods are denoted by the first letter of each respective month)], the sea surface wind stresses are generally weak and SST is warm to the north of 20°S in both the model and the observations (Figs. 2a,b). The observed precipitation is centered at the Sumatra coast and extends southwestward (Fig. 3b). The model precipitation is similar to the observed in general except for a southward bias of the maximum rainfall (Fig. 3a). During boreal summer (JJA), the model reproduces the major features of the atmospheric low-level circulation associated with the Indian summer monsoon, such as the strengthened southeast trade winds, the cross-equatorial atmospheric flow near the African coast, and the southwest winds over the Arabian Sea and the Bay of Bengal (Figs. 2c,d). The monsoon winds cools down the northern ocean generally, and the Somali coast in particular. The model also reproduces the large enhancement of precipitation near the western coast of India and over the Bay of Bengal in this season although the centers of precipitation are slightly biased southward. The observed two rain belts during this season, one in the south and the other in the north, are reasonably well reproduced by the model (Figs. 3c,d). The model also reproduces the retreat of the monsoon in boreal fall (SON; Figs. 2e,f) and the reversed surface winds over the northern ocean in boreal winter (DJF; Figs. 2g,h). A major defect of the simulation, however, is the long lingering of the precipitation near 10°N in boreal fall (Figs. 3e,f). This rain belt is actually enhanced while retreating slowly southward during the next season (Figs. 3g,h). The slow retreat of the rain belt in the north causes the artificial pattern of the double ITCZ during SON and DJF. Suzuki et al. (2004) also show a double ITCZ pattern in the Indian Ocean in DJF from their simulation using a higher-resolution CGCM.

Some background information outside the Indian Ocean relevant to our later discussion is described in the following. The model's mean climatology in the tropical Pacific, though qualitatively realistic, shows a weakened cold tongue in the eastern Pacific and a double ITCZ, which is quite common to the systematic bias of modern CGCMs (e.g., Mechoso et al. 1995). A major deficiency in the model mean seasonal cycle is that a significant semiannual component in the eastern equatorial Pacific causes an early decay of the equatorial cold tongue annually. Interannually, the model generates an ENSO cycle that oscillates on the period around 4–5 yr. A major shortcoming of the ENSO simulation is that an El Niño event is usually peaked in boreal fall instead of winter. Our analysis shows that the unrealistic ENSO phase lock with season is tied to the strong semiannual component of the cold tongue. In fact, a sensitivity experiment, in which a fixed surface heat flux correction is added to the model (Menganello and Huang 2006), shows that both the annual cycle in the eastern Pacific and the ENSO phase lock with season can be improved significantly if the model's mean SST bias is corrected.

An Indonesian Throughflow (ITF) connects the Indian Ocean to the Pacific Ocean in the CGCM with an annual mean transport at 4.23 Sv (1 Sv $\equiv 10^6$ m^3 s^{-1}). This mean transport is within the range of the observation-based estimates but on the weak side (Godfrey 1996). The model transport in the upper 450 m (3.04 Sv) is also lower than the Meyers (1996) measurements of 5 Sv for the upper 400 m using geostrophic currents estimated from repeated expendable bathythermograph (XBT) lines during 1983–94. Seasonally, the model ITF transport in the upper 450 m is weakest in March (2.03 Sv) and strongest in September (4.11 Sv). The maximum transport matches Meyers's (1996) observations but the minimum occurs two months earlier. Interannually, the model ITF transport is more closely related to the ENSO cycle than to the Indian Ocean variability. The model also produces a vigorous southern annular mode, which is seen as the first EOF mode of the seasonally averaged sea level pressure (SLP) anomalies that explains 40% of the total variance. The spatial structure of the mode is similar to the one derived by Gong and Wang (1999) using observational data.

4. Interannual variability

In this section, we analyze the interannual variability of the upper Indian Ocean, using leading modes of the

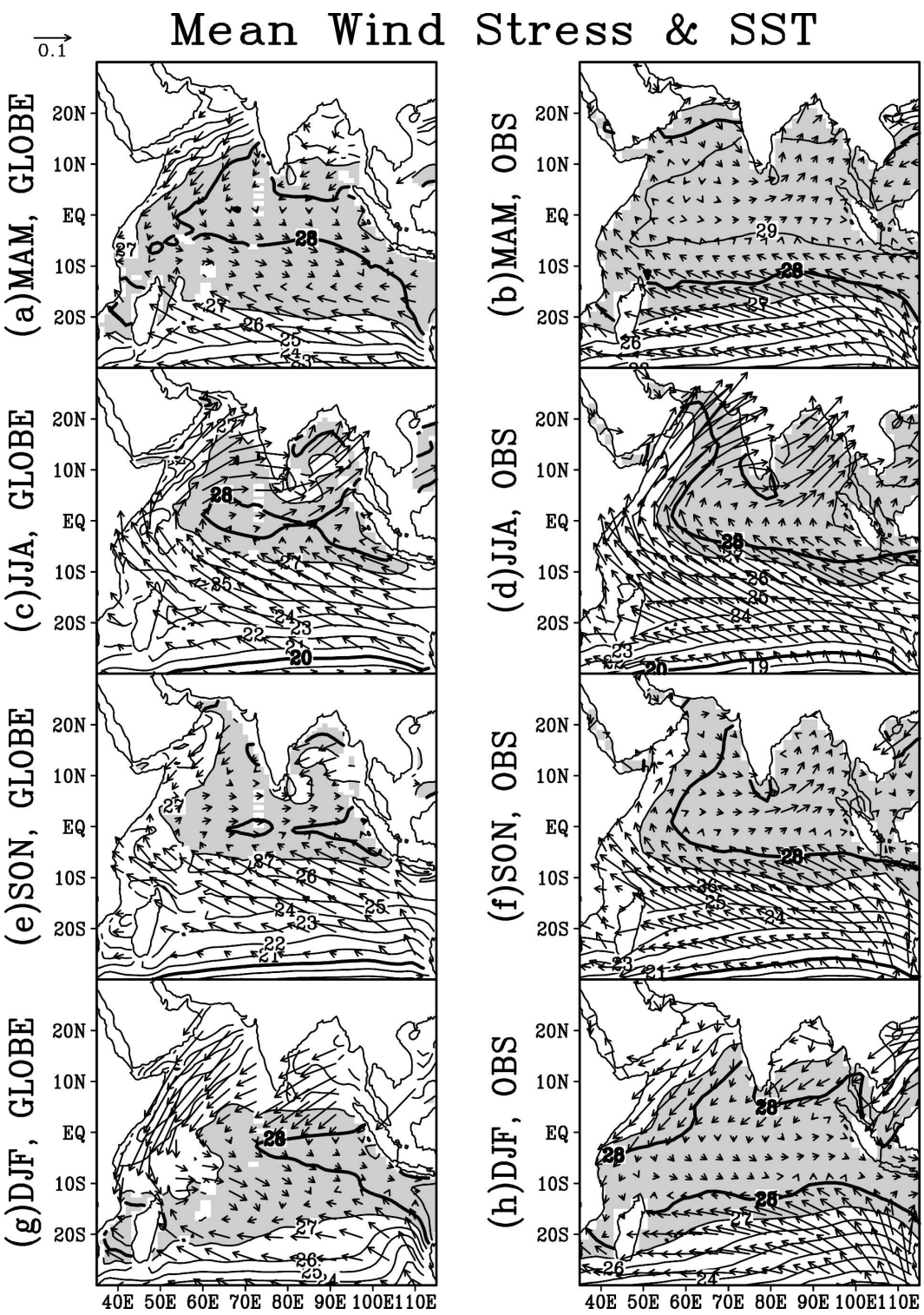

FIG. 2. Mean annual cycle of SST and surface wind stress from (left) the GLOBE simulation and (right) the CPC SST analysis and NCEP–NCAR reanalysis for (a),(b) MAM, (c),(d) JJA, (e),(f) SON, and (g),(h) DJF. The contour interval for SST is 1°C with temperatures greater than 27°C shaded. The scale of surface wind stress for 0.1 N m^{-2} is shown in the upper left corner.

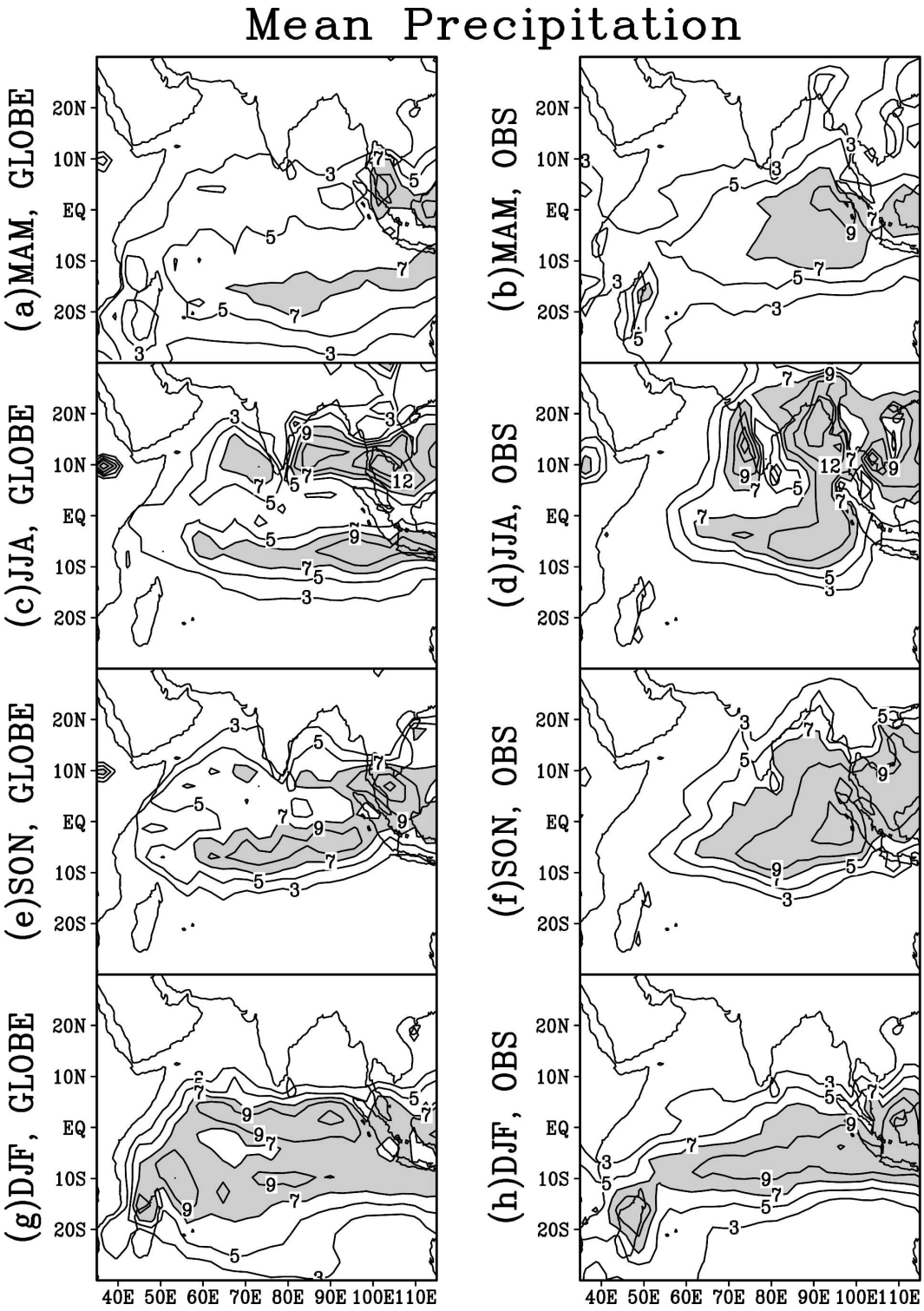

FIG. 3. Mean annual cycle of precipitation from (left) the GLOBE simulation and (right) the CPC analysis for (a),(b) MAM, (c),(d) JJA, (e),(f) SON, and (g),(h) DJF. The contours are at 3, 5, 7, 9, 12, and 15 mm day^{-1}.

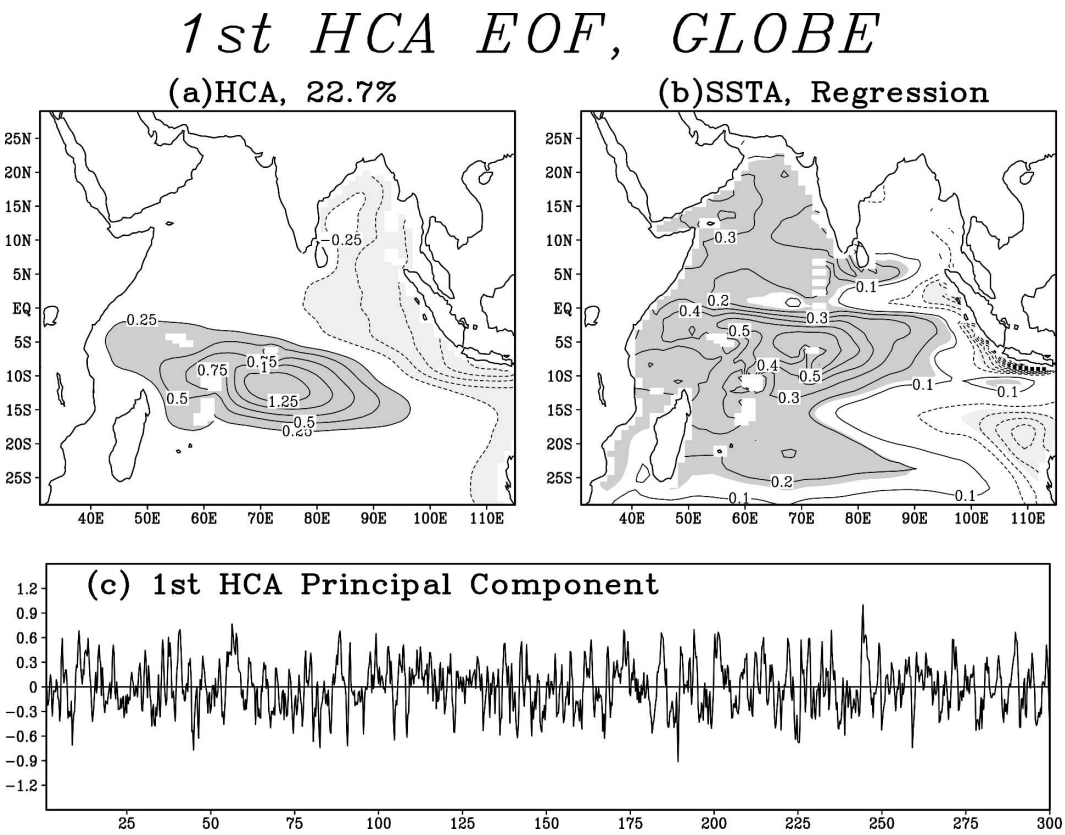

FIG. 4. The first EOF mode of the seasonally averaged HC anomalies in the Indian Ocean from the GLOBE simulation. (a) The spatial pattern of this mode and (c) the principal component. The contour interval in (a) is 0.25°C with zero lines omitted, and regions with HC anomalies larger than 0.25°C (less than −0.25°C) are darkly (lightly) shaded. The principal component is normalized to have maximum magnitude of 1. (b) The regression pattern of the seasonally averaged SST anomalies to the HC principal component in (c). The contour interval is 0.1°C with zero lines omitted, and regions corresponding to the 99% significance level are shaded.

empirical orthogonal functions (EOFs) of the SST and upper-ocean heat content (HC) anomalies from both the GLOBE and CLIM simulations. The HC is defined as the averaged ocean temperature for the upper 275 m. Many previous studies demonstrated that the upper-ocean heat content is a good proxy of the thermocline depth that characterizes the upper-ocean dynamics (e.g., Chao and Philander 1993; Huang and Schneider 1995; Huang and Kinter 2002). Unlike SST, which is strongly linked to the surface heat flux in the Indian Ocean, the HC anomalies are more closely associated with the fluctuations of the surface wind stress and its curl. The simulated HC interannual variability is compared with a 41-yr (1958–98) ocean analysis from a global ocean data assimilation (ODA) system produced by Huang and Kinter (2002) based on observed ocean temperature profiles and SST. The EOF modes are calculated on the domain of the Indian Ocean within 30°S–30°N, 30°–120°E. The chosen domain is the same as that used in our previous observational analysis (Huang and Kinter 2002) so that their results can be compared directly. The seasonal average is used because the SST anomalies in this region generally have a persistence of three to four months.

a. HC variability

Figure 4 shows the first EOF of the seasonally averaged HC anomalies from the GLOBE simulation. The spatial pattern of this EOF (Fig. 4a) is dominated by an elongated anomaly from the southwestern to central Indian Ocean centered at 10°–15°S, 70°E with opposite anomalies extending from the eastern coast into the equatorial Indian Ocean. Its principal component (PC; Fig. 4c) shows a well-defined interannual fluctuation of 3–4 yr with some decadal and longer-term modulation. This HC pattern of oscillation is similar to the first HC EOF mode from the ODA analysis (Fig. 5a). The major model discrepancy is a weak warming in the northwest-

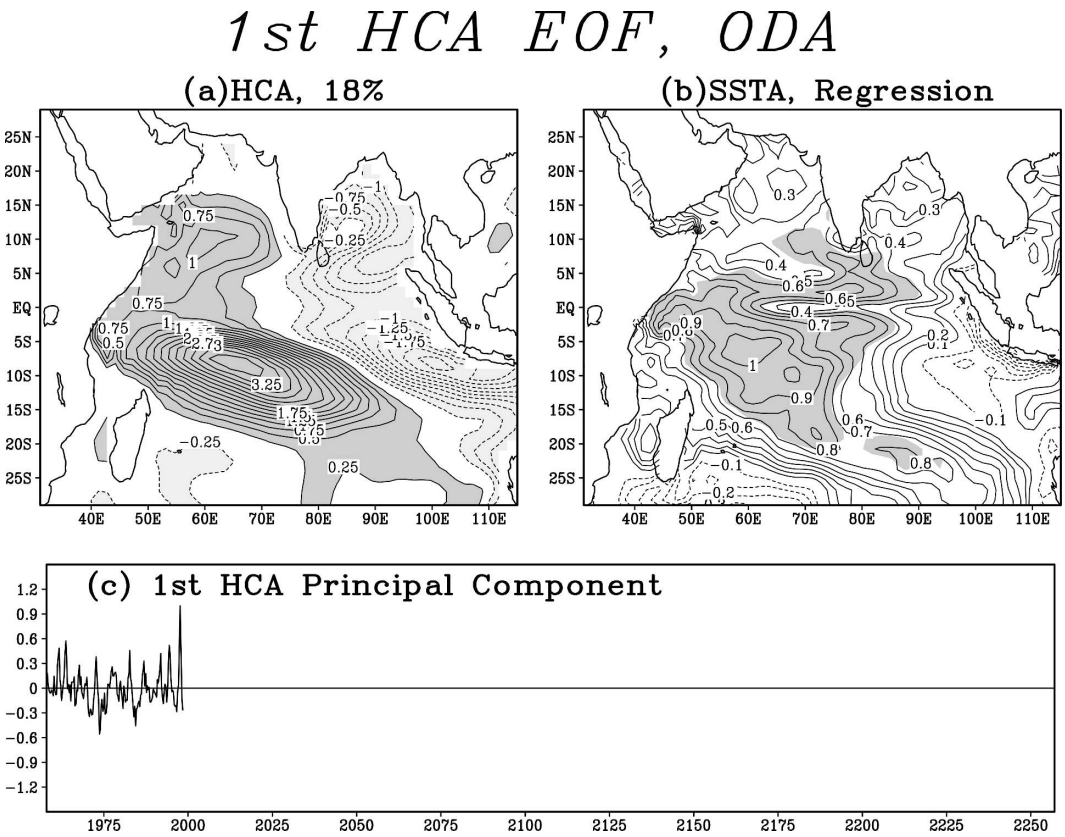

FIG. 5. Same as in Fig. 4, but from the ODA analysis for 1958–98.

ern Indian Ocean. The observed HC pattern also shows larger magnitudes than that in the model (Figs. 4a,b). As we pointed out above, the HC variability mainly represents the low-frequency fluctuation of the thermocline depth as shown in Figs. 1c,e. The vertical structure of the temperature anomalies has been described previously by Murturgudde and Busalacchi (1999) and Annamalai et al. (2003). The barrier layer in the eastern equatorial Indian Ocean due to salinity stratification similar to that described by Masson et al. (2002) for seasonal variability may also play a role in the interannual oscillation.

Figures 4b and 5b show the regressions of the seasonally averaged SST anomalies, respectively, onto the principal components of the first HC modes for the GLOBE run (Fig. 4c) and the observations (Fig. 5c). In both cases, the anomalous SST patterns associated with the HC fluctuations are characterized by a zonal gradient with positive SST anomalies centered near 70°E to the south of the equator and negative anomalies around the Sumatra coast. These patterns are similar to the SST dipole structure described by Saji et al. (1999). In both Figs. 4b and 5b, the SST anomalies are largest within 10° of the equator and most highly correlated to the principal components of the HC EOFs there (not shown). The SST anomalies in the west extend both to the south and north. The correlations of these subtropical SST anomalies to the principal component of the HC mode, however, are lower than those near the equator (not shown). The model also shows too strong cooling near northwestern Australia.

Unlike the forced experiments reported in Part I of this study, the leading HC mode in the GLOBE run is only weakly correlated to the model ENSO cycle. In the GLOBE run, the largest correlation between the HC principal component (Fig. 4c) and the model Niño-3 index[1] is 0.22 when the PC lags Niño-3 for one season, which is also much lower than that from the observations (0.60). The model Niño-3 correlation is statistically significant at the 99% level because of the long record of the simulated data but only explains a small

[1] The Niño-3 index is defined as the regionally averaged SST anomalies within 5°S–5°N, 90°–140°W, which is generally used to characterize the ENSO cycle in the Pacific Ocean in observations. It is also a good indicator of the simulated ENSO cycle by the GLOBE run.

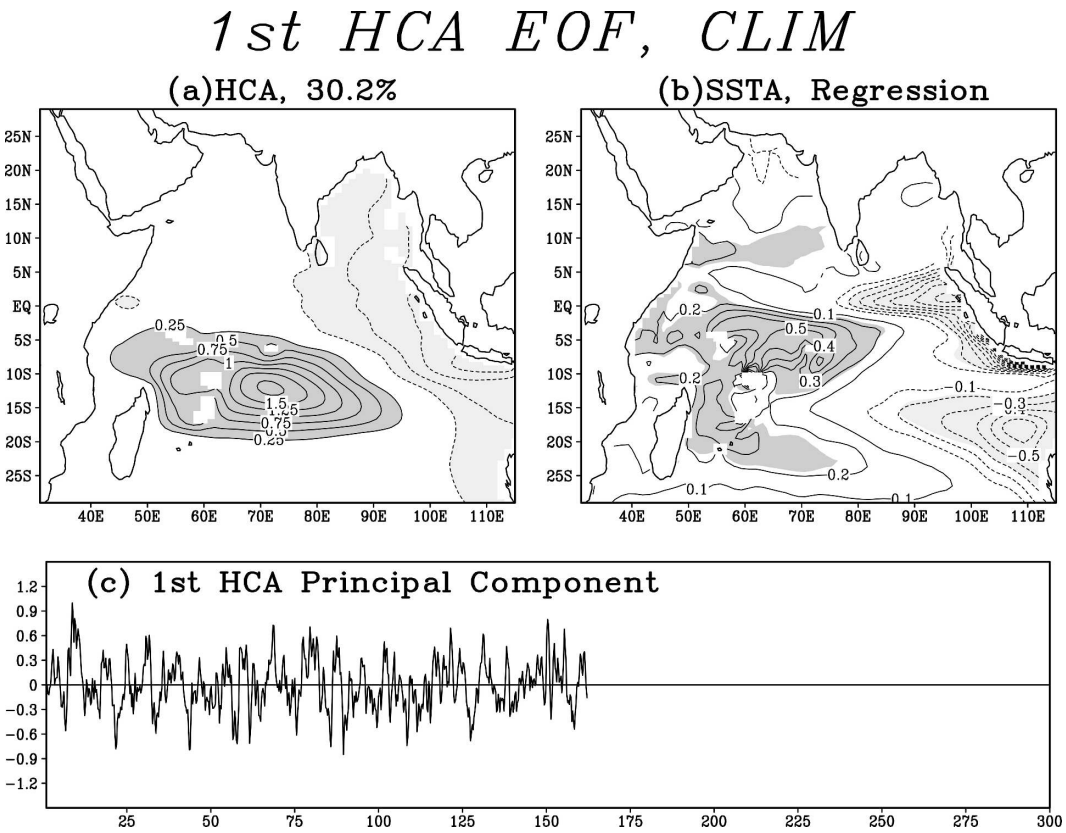

FIG. 6. Same as in Fig. 4, but from the CLIM simulation.

percentage of the total variance. The weaker correlation in the GLOBE run is due to the fact that the ENSO cycle is weaker in the model. The standard deviation of the model Niño-3 index is 0.6°C compared to 0.8°C for the observations based on the SST data from the ODA analysis.

The weaker ENSO forcing, however, does not weaken the model HC pattern significantly. Therefore, the ENSO cycle is not the sole driving force of the HC variability. In fact, even in the CLIM simulation, where ENSO is totally suppressed, the spatial structures of the first HC EOF mode and its SST regression (Figs. 6a,b) are still very similar not only to those in the GLOBE simulation (Figs. 4a,b) but also to those in the observations (Figs. 5a,b). The amplitude of the HC pattern remains strong in the CLIM run partly because the remote influence of the atmospheric internal forcing is intensified when the oceanic domains outside the Indian Ocean basin are uncoupled, as we will show in the next section. However, the similarity of the spatial HC pattern among the simulations with different degrees of ENSO influence suggests that the spatial structure of the thermocline fluctuation in the Indian Ocean is primarily determined by factors within the basin. This pattern is thus an intrinsic feature of the Indian Ocean variability independent of ENSO for its existence.

The air–sea coupling in the Pacific, however, influences some characters of the Indian Ocean HC mode, as shown in the power spectra of the time series of these modes from different runs (Fig. 7). The spectrum of the HC mode from the GLOBE run shows major peaks at 2–3 and 4–5 yr (Fig. 7a), which is roughly consistent with the spectrum of the observation-based ODA HC mode (Fig. 7c). The dominant time scale of the HC oscillation in the GLOBE simulation is close to the model ENSO cycle since the Niño-3 index of the GLOBE run (Fig. 7d), as well as the principal components of the SST and HC first EOF modes of the Pacific basin (not shown), shows a dominant peak near five years. Compared with the observations, the spectral distribution of the model Niño-3 index is generally realistic, except for a slightly lower dominant frequency (not shown). Without air–sea coupling in the Pacific, the power spectrum of the principal component of the CLIM HC EOF (Fig. 7b) shows weakened strength at the band of 4–5 yr and a shift of its major peak to 6–7 yr, consistent with the lower dominant frequency of the oscillation in Fig. 6c.

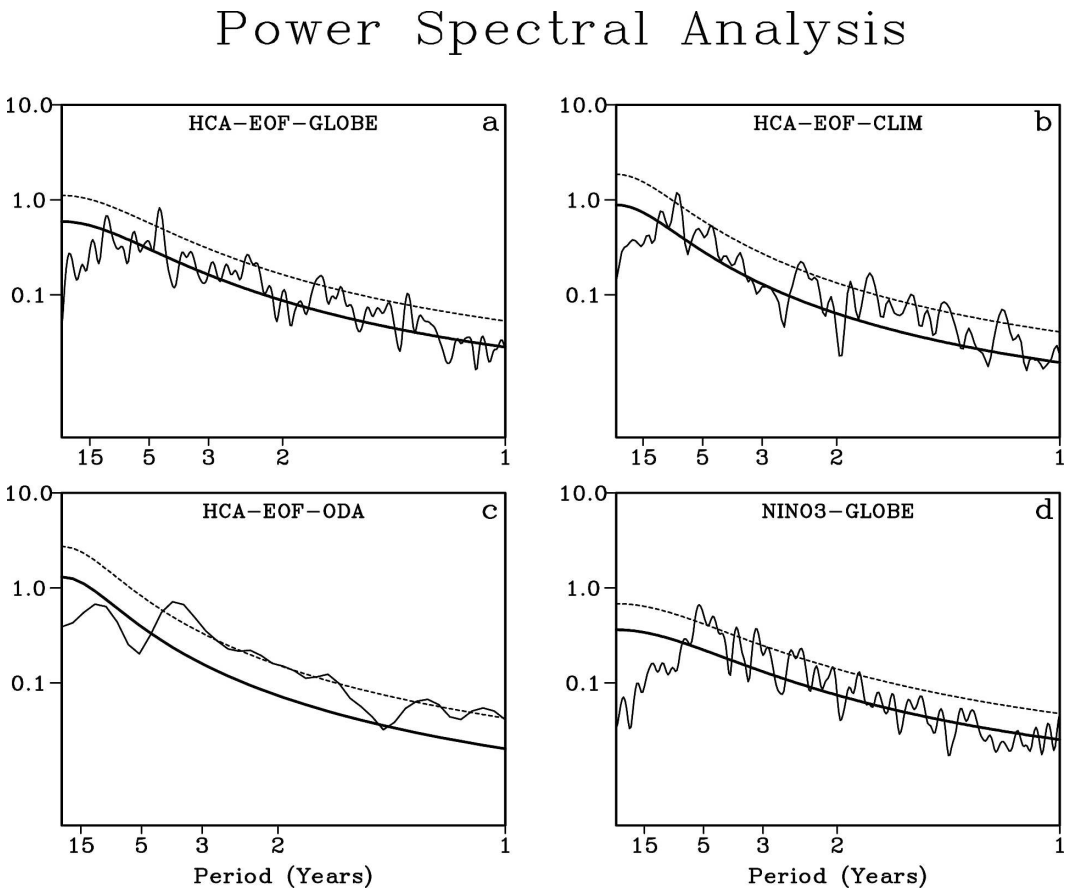

FIG. 7. Power spectra of the principal components of first HCA EOF modes for (a) the GLOBE simulation, (b) the CLIM simulation, and (c) the ODA analysis for 1958–98. (d) The power spectrum of the Niño-3 index from the GLOBE run. The index has been normalized by its maximum magnitude. Within (a)–(d), the thick and dashed curves are, respectively, the expected red noise spectrum and the 95% significance level above the red noise spectrum.

b. SST variability

Apart from the association with the HC anomalies, the SST anomalies are strongly affected by the surface heat flux. As a result, the leading SST EOF patterns are quite different from those shown in Figs. 4b, 5b, and 6b. The latter are more reflective of the dynamical influences of the subsurface anomalies. The first EOF of the ODA SST anomalies for 1958–98 (Fig. 8a) shows a pattern of basinwide warming, with largest SST anomalies occurring over the northern tropical Indian Ocean and extending from the western equatorial ocean southeastward into the southern subtropics. Its time series is highly correlated to the Niño-3 index (0.67) at a lag of one season. This SST pattern is generally attributed to the forcing of the ENSO cycle (Pan and Oort 1990; Kawamura 1994; Lanzante 1996; Wallace et al. 1998). The first SST EOF pattern from the GLOBE simulation (Fig. 8c) qualitatively resembles the observations (Fig. 8a). Its time series also significantly correlated with the model Niño-3 index (0.49) at a lag of one season. It is higher than the HC EOF's correlation to Niño-3, which implies that the model ENSO cycle has a stronger thermodynamical influence on the Indian Ocean than its dynamical influence. Without ENSO forcing, the first CLIM SST EOF (Fig. 8e) explains less total variance than its counterparts in the observations (Fig. 8a) and the GLOBE run (Fig. 8c). In particular, SST anomalies are weak in the northern Indian Ocean in this mode (Fig. 8e). This difference between the two runs implies that these northern SST anomalies are exclusively forced by ENSO-induced surface fluxes.

The second EOF from the observations (Fig. 8b) and simulations (Figs. 8d,f) all show strong SST anomalies centered in the southern subtropical Indian Ocean with two opposite centers characterized by cold SST anomalies off the Australian coast and warm SST anomalies to the southeast of Madagascar. It is different from the

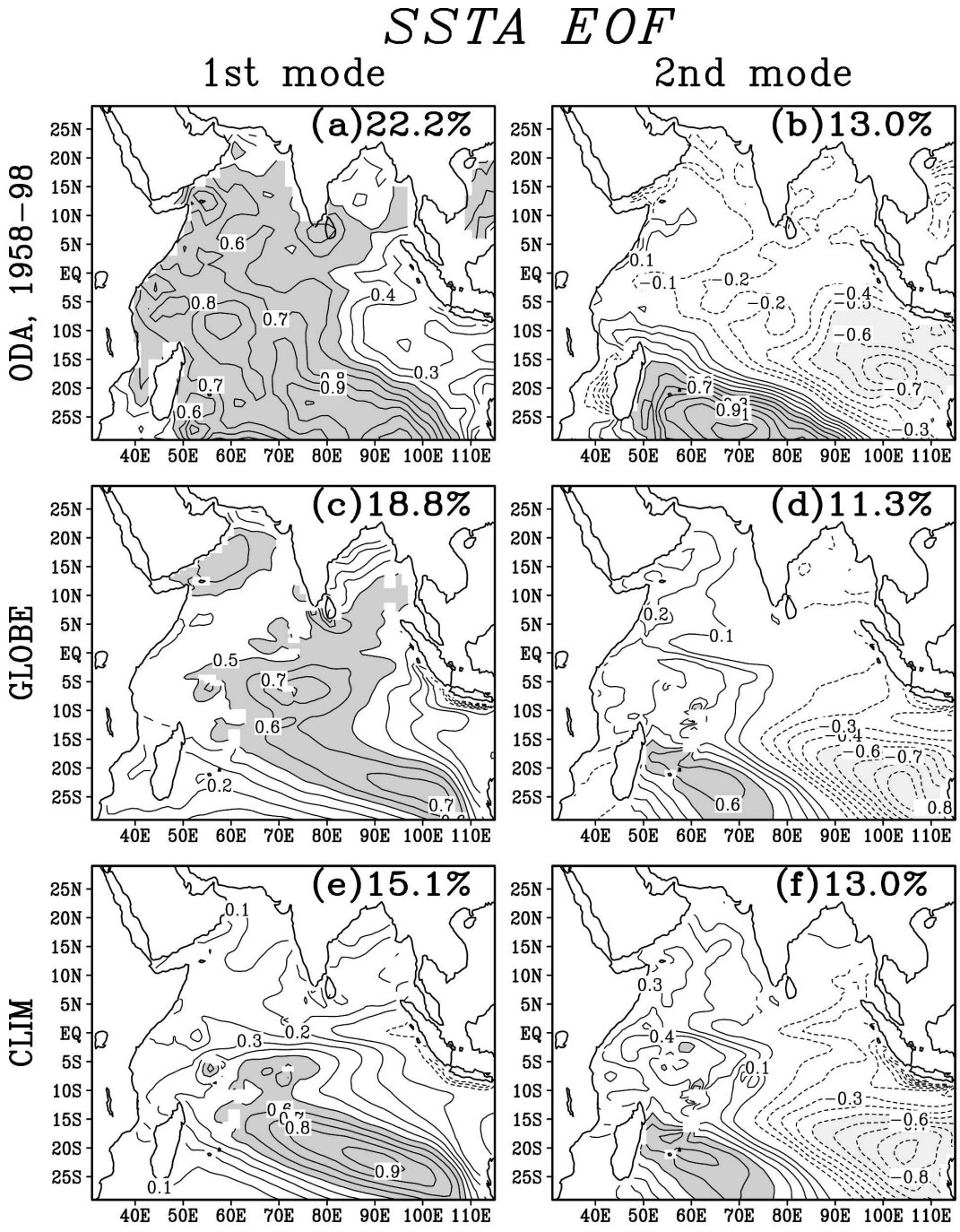

FIG. 8. The spatial patterns of the two leading EOF modes of the seasonally averaged SST anomalies in the Indian Ocean from (a),(b) the observations, (c),(d) the GLOBE simulation, and (e),(f) the CLIM simulation. The first modes are shown in (a),(c),(e) and the second modes in (b),(d),(f). The contour interval is 0.25°C with zero lines omitted. Regions with anomalies larger than 0.5°C (less than −0.5°C) are darkly (lightly) shaded.

SST pattern (Figs. 4b–6b) associated with the HC modes in its more subtropically located centers. Unlike the first SST EOFs, which explain less of the total variance when ENSO is weakened or suppressed, the percentages of the variances explained by the second EOFs are largely unchanged with or without ENSO. The temporal correlations between the second SST EOF and Niño-3 from the observations are around ±0.2 with lags within a year. The corresponding Niño-3 correlations from the GLOBE simulation are all near

zero. One shortcoming of the CGCM-simulated SST variability, as seen from the two leading EOF modes from both runs, is the excessively strong fluctuations close to the Sumatra and Java coasts (Fig. 8). These strong SST anomalies are strictly confined within a narrow zone close to the coast. Their influences are most likely local.

Compared to the leading HC EOF mode, the physical meanings of the two leading SST EOF modes are less obvious, partly because the variance of the SST pattern directly associated with the HC mode is distributed in the first two leading SST EOF modes. The relationship between the leading SST EOF modes and the first HC EOF modes described in the last subsection is also complicated. The largest correlations between the first SST and HC EOF modes are simultaneous in all cases, at 0.54 for the observations, 0.39 for the GLOBE, and 0.21 for the CLIM simulations. The relationships between the second SST and their first HC EOF modes vary from case to case. The observed second SST EOF (Fig. 8b) is uncorrelated with its first HC EOF (Fig. 5a). However, the largest correlation coefficients between the second SST and first HC EOF modes are 0.44 for the GLOBE and 0.49 for the CLIM simulations, respectively. The latter is simultaneous while the former with the SST leading the HC by one season. Moreover, the first and second SST EOFs of the CLIM run do not satisfy the rule of thumb for uniqueness due to the closeness of their explained variances (North et al 1982). This complexity reflects the limitation of the SST EOF analyses in this basin (Hastenrath 2002; Dommenget and Latif 2002). One should be cautious in explaining the physical meaning of each mode separately.

On the other hand, the information derived from the SST EOF analysis, in addition to the result from section 4a, is that there are major SST anomalies in the southern subtropical ocean away from the equatorial waveguide apart from the tropically centered SST anomalies forced by the tropical HC fluctuations. A comparison of the leading SST EOF modes from GLOBE and CLIM experiments also shows that some SST anomalies in the northern tropical Indian Ocean are generated exclusively by remote ENSO forcing. Combining the results from both the HC and SST EOF analyses, we propose that, besides the externally forced SST signals in the northern Indian Ocean, the interannual variability of the tropical Indian Ocean has at least two intrinsic physical patterns. One is the low-frequency dynamical fluctuation of the tropical thermocline depth that contributes to the east–west SST gradient in the equatorial ocean. The other pattern describes the SST fluctuations in the southern subtropical Indian Ocean. We refer to these two patterns as the tropical and subtropical modes, respectively.

To overcome the uncertainties of the statistical analysis in this section, we conducted further analyses to substantiate the existence of these patterns and analyze their physical meanings. Taking the advantage that the Indian Ocean variability shows distinct seasonal dependences (e.g., Saji et al. 1999; Behera and Yamagata 2001; Huang and Kinter 2002; Xie et al. 2002), these examinations are conducted on a season-by-season basis. Moreover, instead of examining the variables separately, we have done multivariate EOF analyses of the HC, SST, and surface wind stress and heat flux anomalies together to see whether their combined patterns are physically meaningful. We also examined the casual relation among the variables through lead–lag regressions and connected the regional modes with global fields to find potential physical triggers outside basin. These studies further suggest the physical existence of these two intrinsic modes. The results of these analyses are summarized in the next two sections.

5. Tropical mode

Figures 9 and 10 show the first multivariate EOF modes of the HC, SST, surface wind stress, and heat flux anomalies in boreal fall (SON) for the GLOBE and CLIM simulations, respectively. The spatial patterns are qualitatively similar between the modes from the two runs for all variables (Figs. 9 and 10). In particular, the HC patterns (Figs. 9a and 10a) are reminiscent of the HC EOF shown in Figs. 4a and 6a, while the SST patterns (Figs. 9b and 10b) show features similar to those depicted in Figs. 4b and 6b. The stronger equatorial easterlies and weaker southeast trade winds in the surface wind stress anomalies are associated with an anomalous anticyclonic circulation of the surface wind stress (Figs. 9c and 10c), which forces the HC anomalies to the south of the equator shown in Figs. 9a and 10a. The surface heat fluxes (Figs. 9d and 10d) generally damp the dynamically generated SST anomalies in the equatorial zone, while the weakened southeast trade winds reduce the net heat loss in the subtropics. Overall, this mode is dominated by the dynamical air–sea feedback among the anomalies of the surface wind stress, HC, and SST, which characterizes the tropical mode of the Indian Ocean. Similar patterns appear as the first modes in boreal winter (DJF) in both runs (not shown). Temporally, the fall and winter modes are highly correlated with each other in both runs, suggesting a continuous evolution of the tropical air–sea anomalies with seasons.

In the next two subsections, we study the seasonal

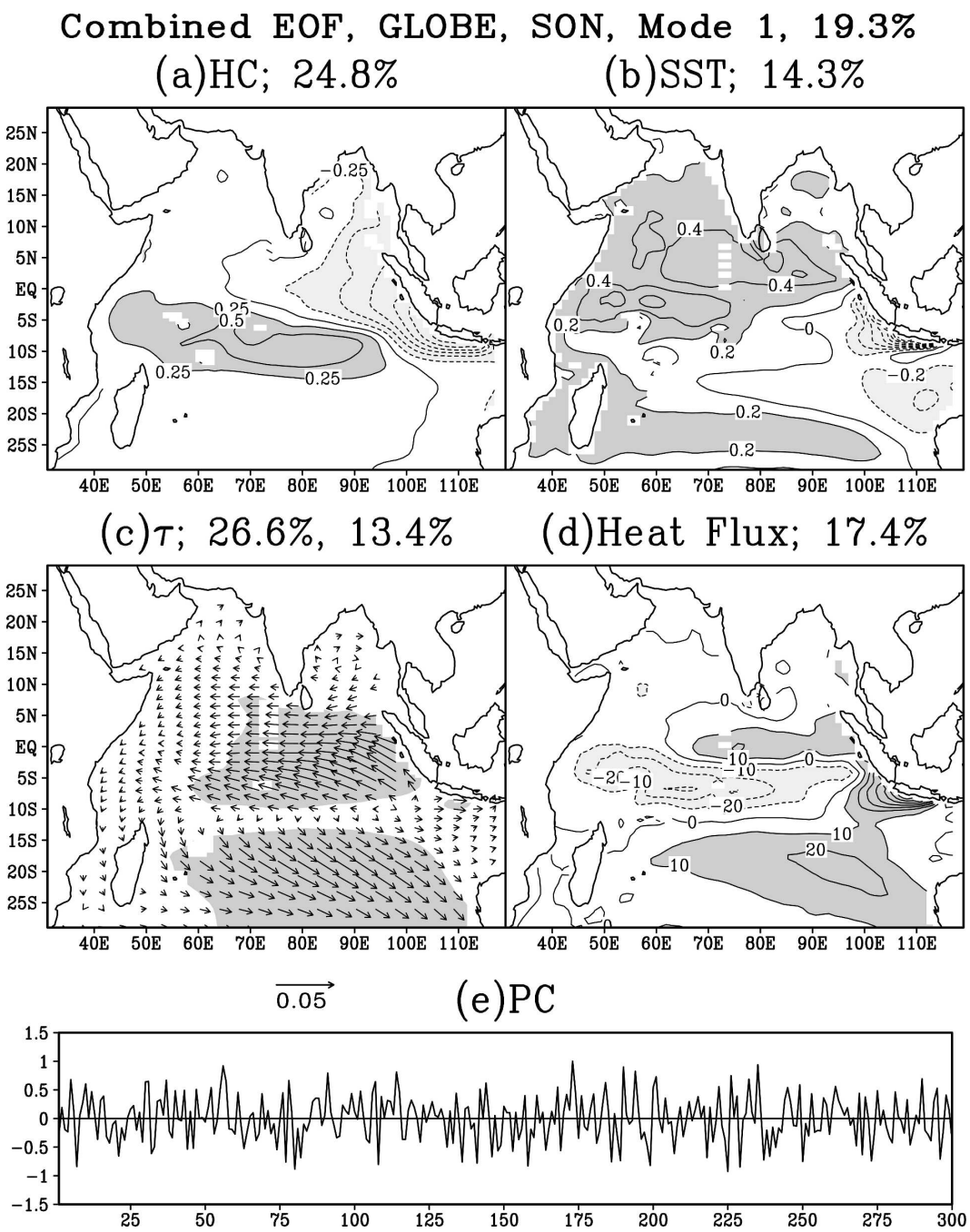

FIG. 9. The first multivariate EOF mode for SON from the GLOBE simulation. The spatial patterns are for (a) HC, (b) SST, (c) wind stress, and (d) net surface heat flux anomalies; (e) the principal component. The contour intervals are 0.25°C for HC in (a), 0.2°C for SST in (b), and 10 W m^{-2} for the heat flux in (d). The vector of 0.05 N m^{-2} is shown below (c) for surface wind stress. The dark (light) shadings in (a),(b),(d) show HC anomalies larger than 0.25°C (less than −0.25°C), SST anomalies larger than 0.2°C (less than −0.2°C), and surface heat flux anomalies larger than 10 W m^{-2} (less than −10 W m^{-2}), respectively. The shading in (c) shows the areas of wind stress magnitude larger than 0.01 N m^{-2}. The percentage explained by this combined mode to the total combined variance is given in the title. The percentage of variance explained for each variable by its corresponding pattern is given in the title of its panel.

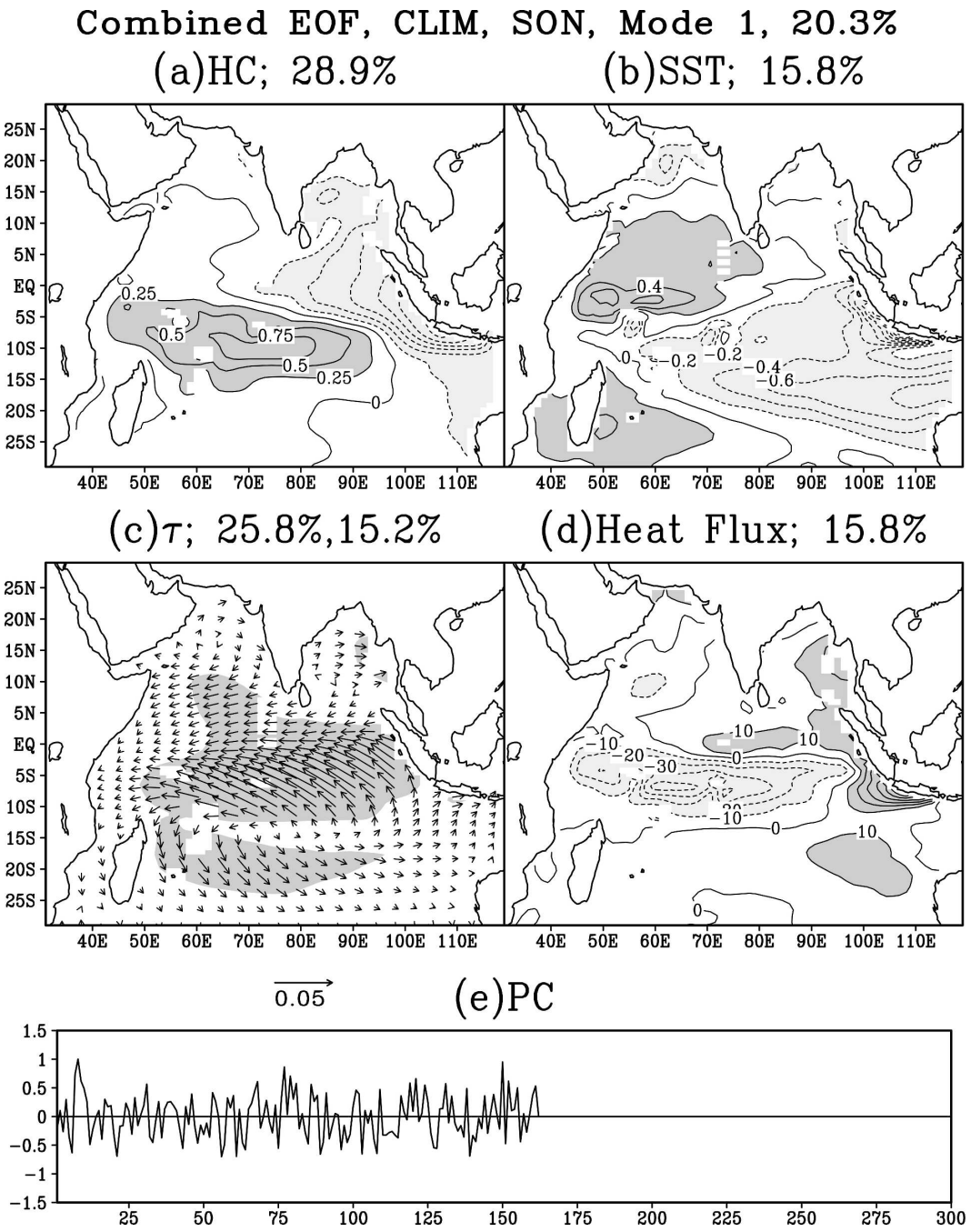

FIG. 10. Same as in Fig. 9, but from the CLIM simulation.

evolution of this mode from boreal summer to winter. We also show the relationship between the tropical mode and the ENSO cycle in the GLOBE run and examine the regional processes that are more closely associated with the tropical mode in the CLIM run.

a. ENSO influence

As shown by the ensemble simulation, the prescribed observational SST anomalies associated with the El Niño events can remotely force an anomalous anticyclonic atmospheric surface circulation over the southern tropical Indian Ocean from late boreal summer to winter, which forces an air–sea pattern similar to those shown in Figs. 9 and 10 (Huang and Shukla 2007). Therefore, the observed ENSO cycle plays a major role in forcing the fluctuation of the Indian Ocean tropical mode. Here we further demonstrate that some of the relationship is preserved in the GLOBE run even

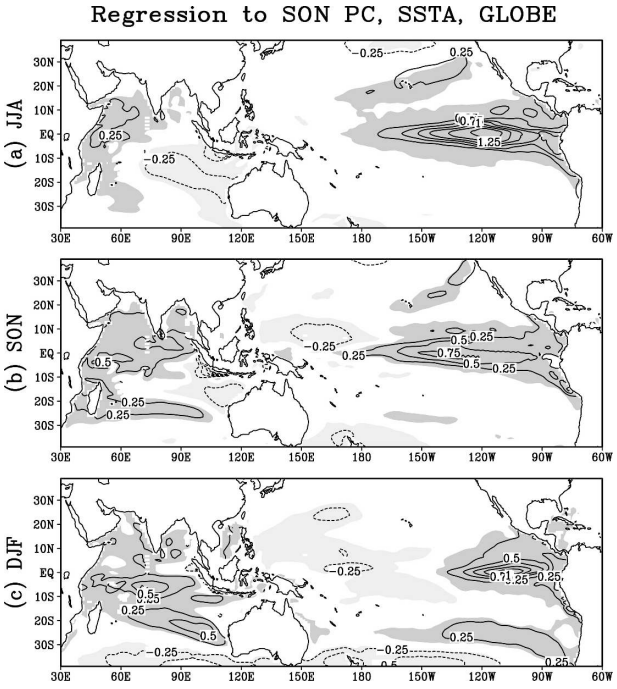

FIG. 11. The regression coefficients of the PC of the first SON multivariate EOF mode from the GLOBE simulation on the seasonally averaged SST anomalies in (a) JJA, (b) SON, and (c) DJF. The contour interval is 0.25°C. The regions above the 99% significance level are shaded.

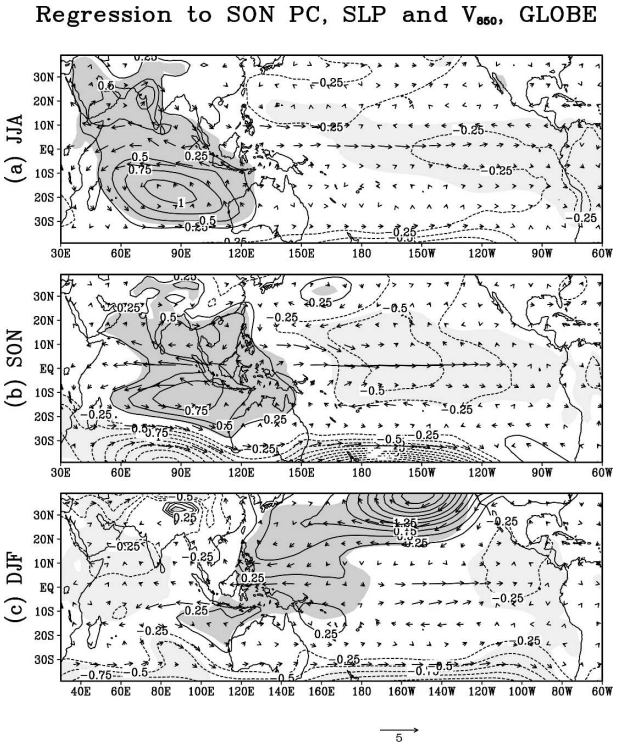

FIG. 12. The regression coefficients of the PC of the first SON multivariate EOF mode from the GLOBE simulation on the seasonally averaged SLP and 850-hPa wind anomalies in (a) JJA, (b) SON, and (c) DJF. The contour interval of the SLP anomalies is 0.25 hPa and the zero lines are omitted. The regions with SLP anomalies above the 99% significance level are shaded. The wind regression is presented in vector form with the scale of 5 m s^{-1} shown at the bottom of the figure.

though the model ENSO is weaker. We also notice that the model ENSO deficiency influences the simulation of the tropical mode in the Indian Ocean.

Compared to the HC EOF pattern for all seasons, the coupled tropical mode in the GLOBE simulation for SON is more significantly correlated to the ENSO cycle, with the highest correlation coefficient of 0.44 when the Niño-3 index leads for one season. Figure 11 presents the regression coefficients of the SST anomalies in the Indo-Pacific basin on the principal component of the SON combined EOF for boreal summer, fall, and winter. It shows that the evolution of the tropical Indian Ocean mode is connected to the El Niño in the Pacific. When the warming is developed in the eastern equatorial Pacific in boreal summer (JJA), warm SST anomalies appear in the western Indian Ocean with cold anomalies in the east centered at the Sumatra and the Australian coasts (Fig. 11a). In the next season, the zonal SST gradient is further developed in the equatorial Indian Ocean while most of the northern Indian Ocean is warmed up (Fig. 11b). By boreal winter (DJF), the whole Indian Basin is warm, with the strongest warming in the central Indian Ocean just to the south of the equator (Fig. 11c), which is partly a response to the deepened thermocline started a season before (Fig. 9a). Moreover, a belt of SST anomalies extends from the equatorial ocean southeastward as shown in the leading mode of the SST EOF (Fig. 8c). This belt is forced by the anomalous trade wind–induced surface heat flux from the previous season (Figs. 9c,d). The pattern in DJF is consistent with the pattern of ENSO influence in the Indian Ocean as shown in Wallace et al. (1998). It is also consistent with Xie et al.'s (2002) earlier finding that tropical SST anomalies generate substantial SST anomalies in the subtropical ocean.

Figure 12 shows the regressions of the principal component of the multivariate EOF from the GLOBE run (Fig. 9c) onto the anomalies of sea level pressure (SLP) and 850-hPa wind. The regression pattern of the precipitation anomalies is shown in Fig. 13. During boreal summer of an El Niño year, an anomalous high SLP is established in the Indian Basin with centers in both the north and south (Fig. 12a), which weakens the Indian monsoon but increases the precipitation near the equator (Fig. 13a). The westward shift of precipitation occurs in the equatorial Indian Ocean during boreal fall

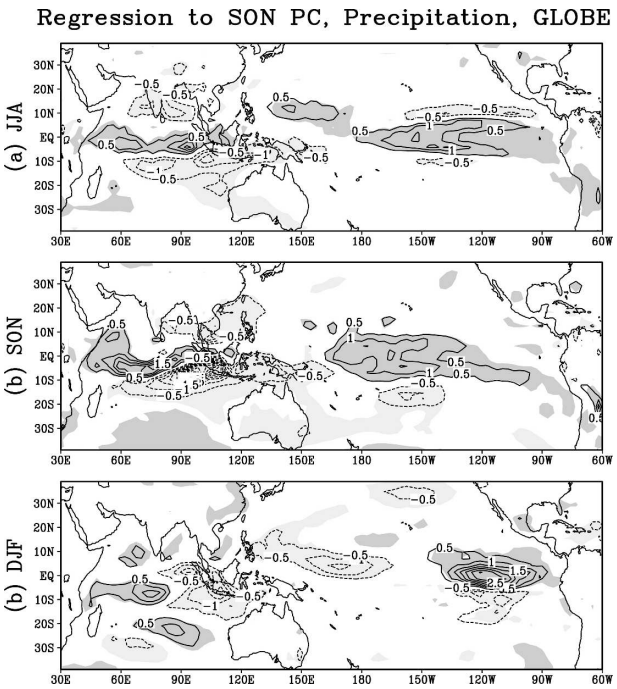

FIG. 13. Same as in Fig. 11, but on the seasonally averaged precipitation anomalies. The contour interval of the precipitation is 1 mm day^{-1}.

(Fig. 13b) while the zonal SST gradient is established there (Fig. 11b). This process of ENSO influence is consistent with the scenario described by Huang and Shukla (2007) under prescribed SST forcing in the Pacific.

The amplitude of the anomalous anticyclone in the southern tropical Indian Ocean starts to weaken in boreal fall (Fig. 12b) and, by the winter, only its remnants exist near the Australian and the southern Sumatra coasts (Fig. 12c). This deviates from the observations and the model ensemble simulation's response to the observed ENSO forcing when the anomalous anticyclone reaches its peak strength in boreal winter (Huang and Kinter 2002; Huang and Shukla 2007). This difference is caused by an early decay of the model El Niño events when the warm Pacific SST anomalies start to weaken on the equator in boreal fall (Fig. 11b) and shift eastward in the winter (Fig. 11c). As described in section 3, the early decay of the El Niño events in the Pacific is strongly associated with the systematic bias of the model mean state and annual cycle. The ENSO influence on the Indian Ocean tropical mode, though with realistic structure, is much weaker in the GLOBE simulation than in the observations because the model ENSO cycle is weaker and less persistent. Combining the result of the GLOBE run and the ensemble simulation, we conclude that the ENSO strength and duration are major prerequisites for affecting the tropical Indian Ocean mode effectively.

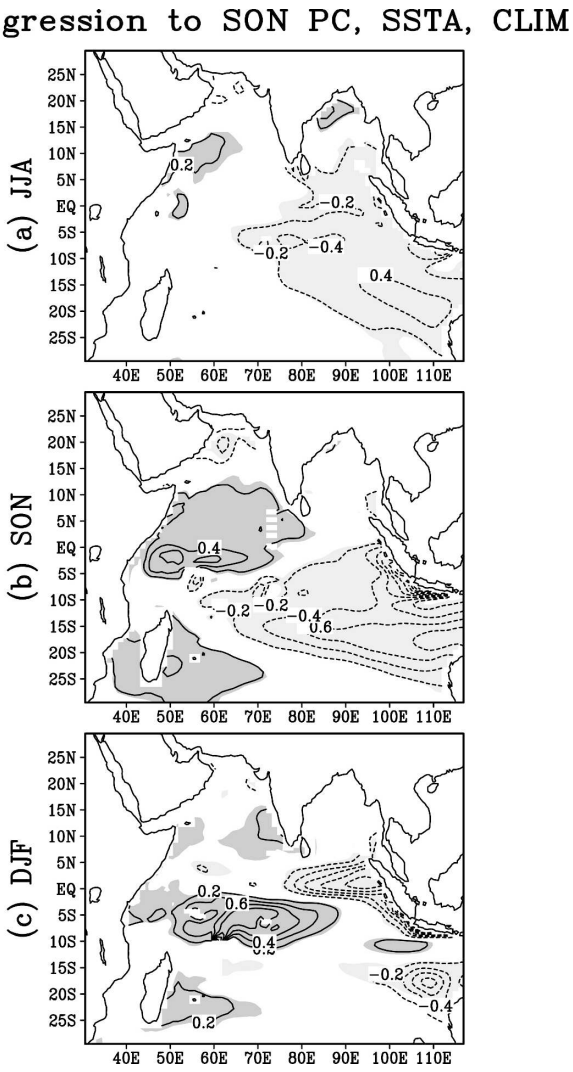

FIG. 14. Same as in Fig. 11, but from the CLIM simulation.

b. Connection to the western Pacific monsoon

Apart from ENSO, the vigorous tropical oscillation in GLOBE is associated with other external influences. The CLIM experiment further isolates these influences. Figure 14 shows the regression patterns of the seasonal mean SST anomalies onto the PC of the first multivariate EOF mode in SON from the CLIM run (Fig. 10e). The corresponding regression patterns for SLP and 850-hPa wind anomalies are shown in Fig. 15 and the patterns for rainfall anomalies in Fig. 16. In the absence of ENSO, the anomalous events in the Indian Ocean are usually initiated by the cooling in the eastern equatorial and southern Indian Ocean during the boreal

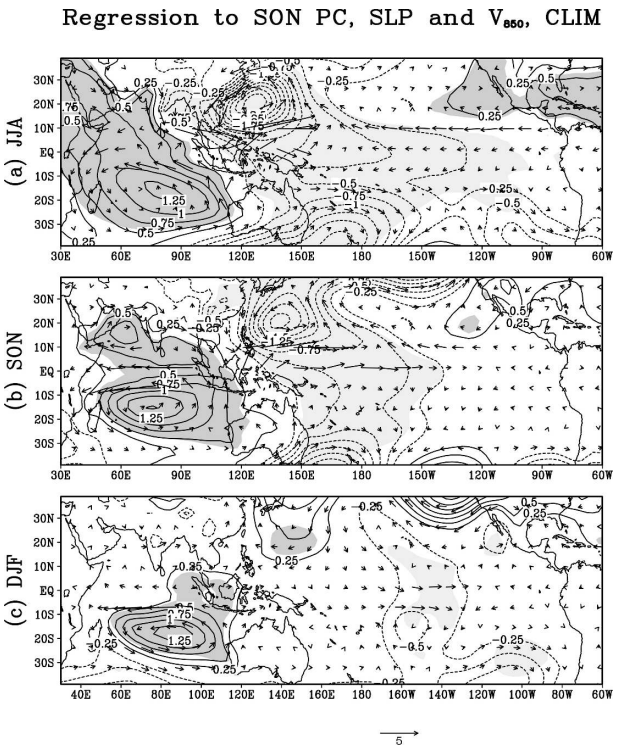

FIG. 15. Same as in Fig. 12, but from the CLIM simulation.

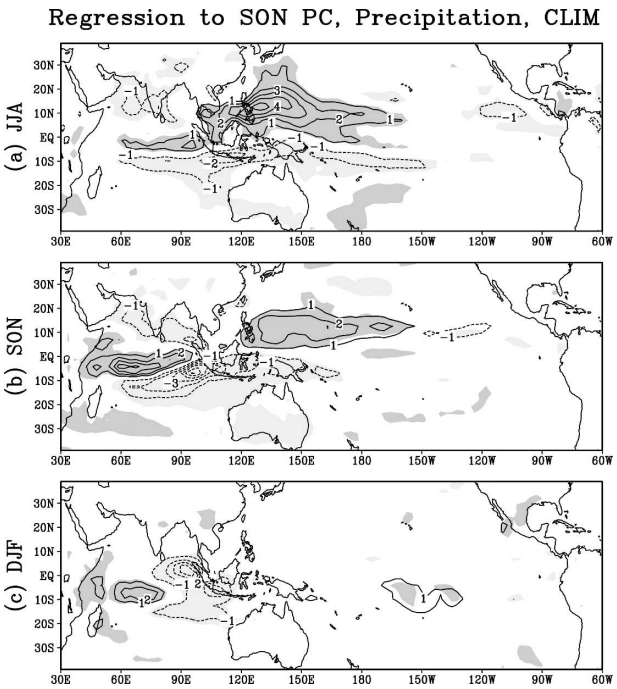

FIG. 16. The regression coefficients of the PC of the first SON multivariate EOF mode from the CLIM simulation on the seasonally averaged precipitation anomalies in (a) JJA, (b) SON, and (c) DJF. The contour interval is 1 mm day^{-1}. The regions above the 99% significance level are shaded.

summer while the warming in the west is weaker (Fig. 14a). As in the GLOBE case, the cooling is associated with an anomalous anticyclonic circulation pattern in the Indian Ocean centered at about 20°S and 90°E (Fig. 15a). This Indian Ocean anticyclonic pattern is accompanied by a widespread cyclonic circulation over the uncoupled domain centered in the northwestern Pacific at about 10°N and 140°W. Consistent with the circulation pattern, positive rainfall anomalies occur near the equator around the low SLP center in the northwestern Pacific while rainfall deficit occurs farther south from the Indian Ocean into the western Pacific (Fig. 16a), which is consistent with Kajikawa et al.'s (2003) anomalous pattern of the outgoing longwave radiation in July preceding an Indian Ocean dipole event (their Fig. 11). Kajikawa et al. (2003) suggest that these meridionally asymmetric convective anomalies during boreal summer are caused by an anomalous Hadley cell over the western Pacific between the marine continent and the South China Sea/Philippine Sea. This direct thermal cell enhances the southeast trade winds over the southeastern equatorial Indian Ocean. The enhanced low SLP center and precipitation in the northwestern Pacific also occur in the boreal summers that precede the Indian Ocean anomalous events in the ENSO-forced ensemble simulation (Part I) and, to a lesser extent, the GLOBE simulation (Figs. 12a and 13a).

Once initiated, the evolution of the zonal SST gradient (Fig. 14b) and rainfall shift (Fig. 16b) within the Indian Ocean in the next season is similar to those in the GLOBE case. The major difference is that there are no significant basinwide warming and southward extension of the SST anomalies in boreal winter (Fig. 14c). The lack of warming in the southern subtropical ocean is related to the westward shift of the anticyclone in boreal fall (Fig. 15b), causing weaker wind and heat flux anomalies over the central ocean (Figs. 10c,d). These ENSO-independent Indian Ocean events remotely generate sizable zonal wind anomalies over the western and central equatorial Pacific Ocean during boreal fall (Fig. 15b), which shift eastward in boreal winter (Fig. 15c). It has significant implication for the evolution of the Pacific ENSO cycle. Seasonally, the appearance of the Indian Ocean–generated equatorial wind over the equatorial Pacific in boreal fall and winter is too late to play a major role in initiating the ENSO events. However, since an Indian Ocean warm event is usually generated as a response to a developing El Niño in the Pacific in reality, these Indian Ocean–induced wind anomalies actually enhance the El Niño development and prolong the Pacific anomalies (Kirtman and Shukla 2000; Annamalai et al. 2005). The significantly

enhanced El Niño condition in the late fall and winter in turn strengthens the anticyclonic surface circulation over the southern tropical Indian Ocean that maintains the anomalous thermocline pattern there. Potentially, the mutual enhancement or positive feedback can prolong the anomalous conditions in both oceans.

In the absence of ENSO, the coupled oscillation in the CLIM simulation is either caused by air–sea interactions within the tropical Indian Ocean or triggered by atmospheric internal fluctuations. One trigger is the anomalous cyclone over the tropical northwestern Pacific, which shows strong rainfall anomalies during boreal summer before the surface anticyclone is fully developed over the Indian Ocean. Since the SST is fixed to its monthly climatology in the Pacific, these atmospheric anomalies are internally generated. Through a regional direct thermal cell, the anomalous cyclone in the northwestern Pacific causes strong subsidence over the southeastern Indian Ocean. It induces an anticyclonic response in the Indian Ocean and perturbs the precipitation near the Sumatra coast remotely because the latter is connected to the atmospheric convection over the warm pool. These anomalies in the Pacific are associated with the fluctuations of the northwestern Pacific monsoon (Murakami and Matsumoto 1994; Wang et al. 2001), which persist in the CLIM simulation for more than a season without local SST change.

The long persistence of the SLP/precipitation anomalies in the northwestern Pacific without local air–sea feedback is similar to the situation shown by Goswami et al. (1984) for an uncoupled AGCM, in which a disturbance to a precipitation center near the equator can persist for a long time even without external forcing. In comparison with the GLOBE simulation (Fig. 12a), the lack of coupling in the northwestern Pacific in the CLIM run actually enhances the local SLP anomalies during JJA (Fig. 15a). Therefore, the influence of the northwestern tropical Pacific monsoon on the tropical Indian Ocean fluctuation is enlarged in the CLIM simulation compared to the GLOBE run.

6. Subtropical mode

The subtropical mode is characterized by the first multivariate EOF mode for the GLOBE run in austral fall (MAM), as shown in Fig. 17. This mode explains 17% of the total variance. The first multivariate EOF mode of the CLIM run for this season gives very similar patterns for all variables (not shown). The SST pattern of the GLOBE mode (Fig. 17b) shows an east–west dipole in the southern subtropics as depicted by the second SST-only EOF modes (Fig. 8d). This SST pattern is forced by the anomalous surface heat gain and loss (Fig. 17d). The heat flux anomalies are in turn generated by wind speed anomalies in the subtropical ocean (Fig. 17c) associated with a dominant cyclonic circulation in the central and western basin centered at 25°S and 65°E with a weaker anticyclone to its east.

At the northern tip of the anomalous cyclone, the northwesterly surface wind anomalies generate northeastward Ekman transport (Fig. 17c) and force positive HC anomalies in the southwestern Indian Ocean centered at 10°–15°S and 60°–70°E (Fig. 17a). These subtropical HC anomalies account for much less percentage of the total HC variance in MAM than does its tropical counterpart located farther north in SON (Fig. 9a). Therefore, the subtropical mode is primarily a thermodynamic process. As we will see later, the subtropical HC anomalies enhance the persistence of the local SST anomalies to the following season.

Figure 18 shows the regression patterns between the principal component of the subtropical mode from the GLOBE run (Fig. 17e) and the SLP and SST anomalies from austral summer (DJF) to winter (JJA). The pattern of the SST anomalies in the subtropical Indian Ocean as shown in Fig. 17b is preceded by a significant deepening of the Antarctic surface pressure accompanied by an increase of the SLP over the circumpolar belt between 40° and 60°S (Fig. 18a). This is the typical pattern of the positive phase of the Antarctic oscillation or the southern annular mode as described by Gong and Wang (1999) and Thompson and Wallace (2000). The positive southern annular mode intensifies the surface westerlies over the circumpolar ocean. Within the anomalous high SLP belt, anticyclonic centers are formed in the central parts of the South Pacific, Atlantic, and Indian Oceans. In the South Indian Ocean, high SLP anomalies extend northwestward into the eastern Indian Ocean along the southwestern Australian coast. Downstream of this anomalous subtropical high in the east, a weak low SLP center is developing off the eastern coast of Madagascar.

The SST pattern in this season (Fig. 18b) shows that, in the extratropical Southern Ocean, cold SST anomalies form a near-circumpolar ring largely under the negative SLP anomalies while the warm SST anomalies formed farther north, especially under or near the major anticyclonic centers. This SST pattern is associated with anomalous upwelling along the margins of the Antarctic continent forced by the northward Ekman transport in the circumpolar ocean and downwelling at midlatitudes associated with the convergence of the Ekman transport (Hall and Visbeck 2002). In the subtropical ocean, the northward extension of the anomalous SLP ridge strengthens the southeast trade winds in its southern flank, which increases the evaporative heat

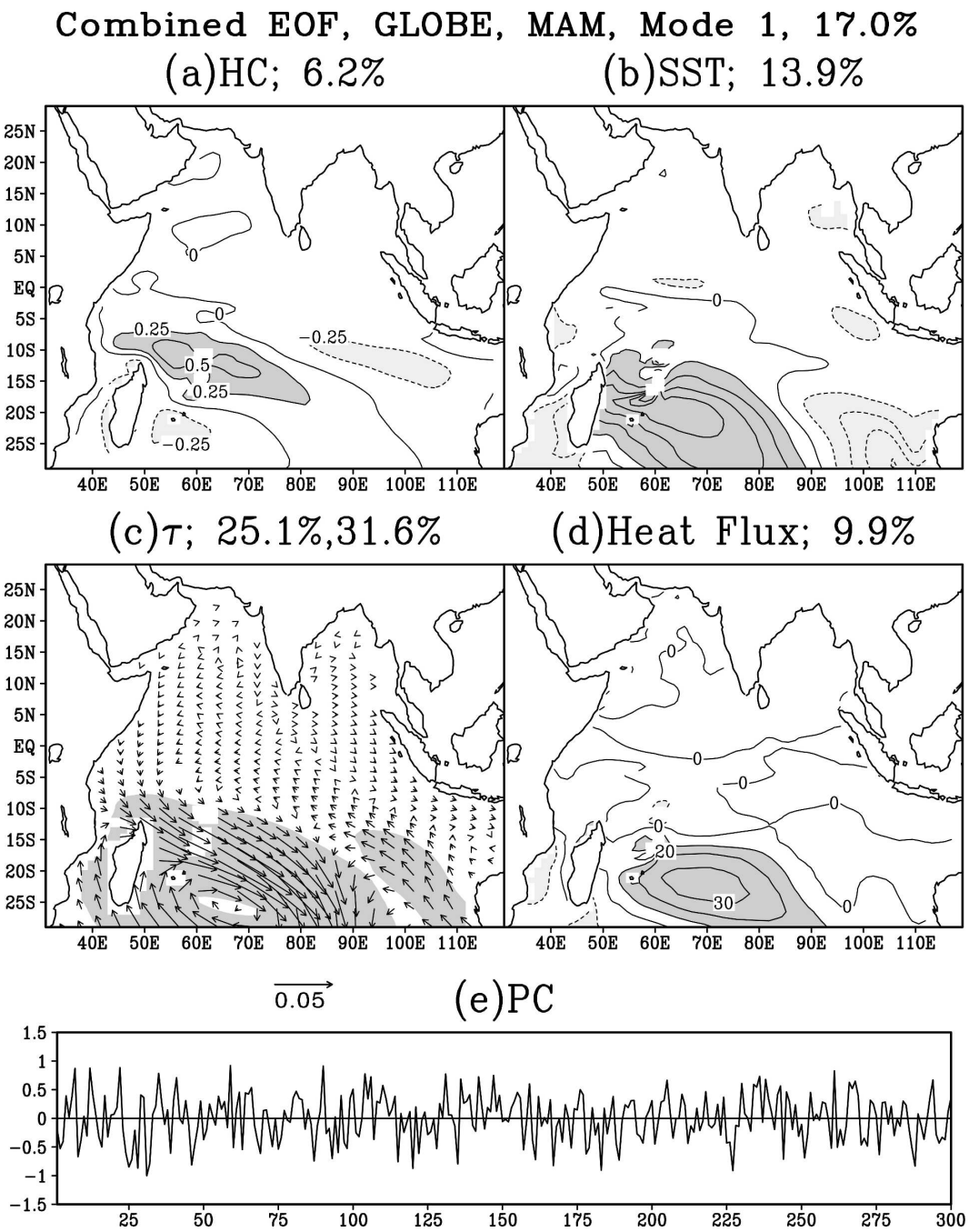

FIG. 17. The first multivariate EOF mode for March-April-May (MAM) from the GLOBE simulation. The spatial patterns are for (a) HC, (b) SST, (c) wind stress, and (d) net surface heat flux anomalies; (e) the principal component. The contour intervals are 0.25°C for HC in (a), 0.2°C for SST in (b), and 10 W m^{-2} for the heat flux in (d). The vector of 0.05 N m^{-2} is shown below (c) for surface wind stress. The dark (light) shadings in (a),(b),(d) show HC anomalies larger than 0.25°C (less than −0.25°C), SST anomalies larger than 0.2°C (less than −0.2°C), and surface heat flux anomalies larger than 10 W m^{-2} (less than −10 W m^{-2}), respectively. The shading in (c) shows the areas of wind stress magnitude larger than 0.01 N m^{-2}. The percentage explained by this combined mode to the total combined variance is given in the title. The percentage of variance explained for each variable by its corresponding pattern is given in the title of its panel.

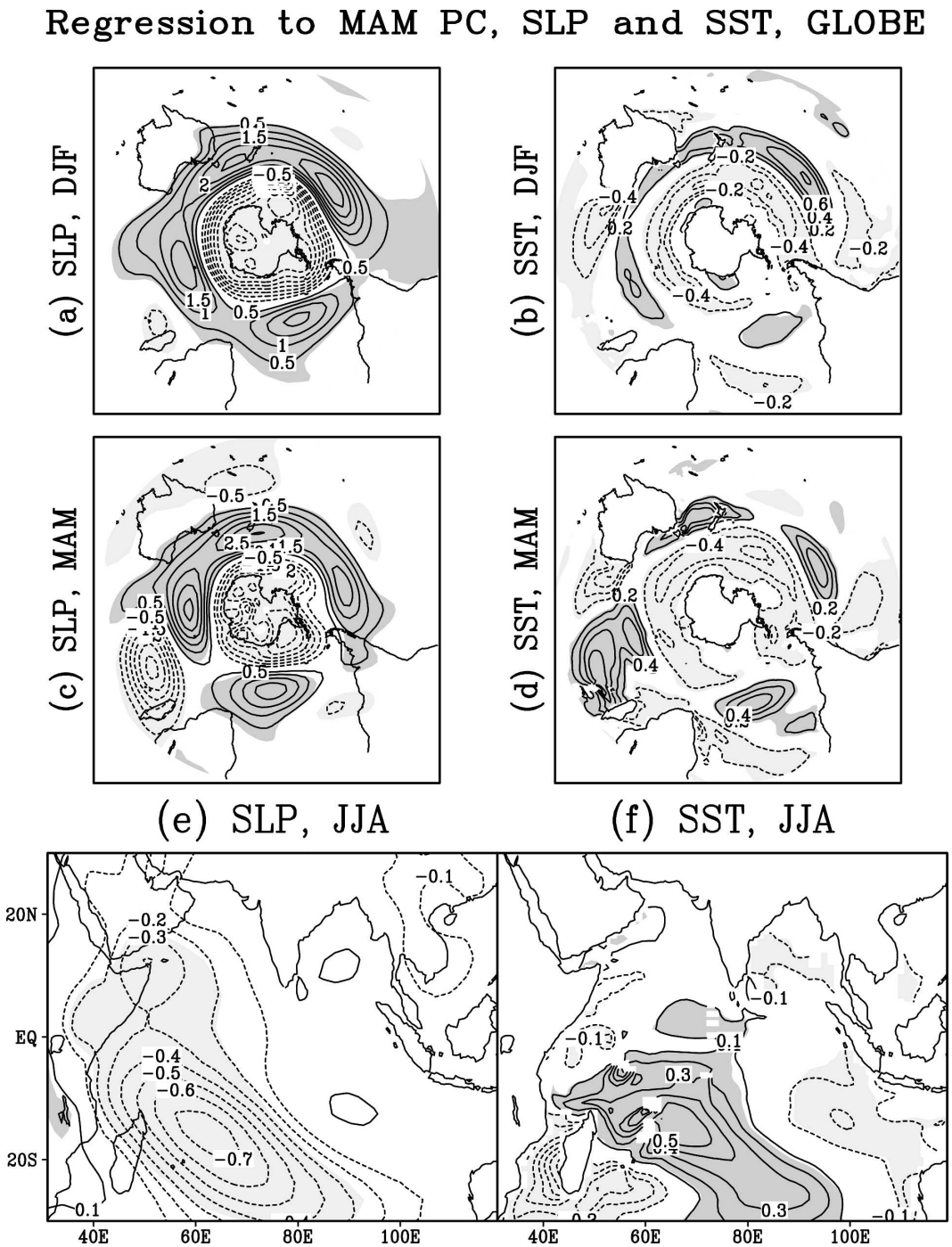

FIG. 18. The regression coefficients of the PC of the first MAM combined EOF mode from the GLOBE simulation to the seasonally averaged anomalies of the (a),(c),(e) SLP and (b),(d),(f) SST in (a),(b) DJF, (c),(d) MAM, and (e), (f) JJA. The contour intervals of the SLP are 0.5 hPa in (a) and (c) and 0.1 hPa in (e). The contour intervals for SST are 0.2°C in (b) and (d) and 0.1°C in (f). The regions above the 99% significance level are shaded.

loss from the sea surface and generates cold SST anomalies locally.

The anomalous Antarctic SLP low is sustained into the austral fall (MAM) while the subtropical high centers are generally enhanced and shifted eastward (Fig. 18c). Within the Indian Ocean, the anomalous low SLP center over the western Indian Ocean, which was weak and barely significant statistically during the previous

season (Fig. 18a), deepens rapidly (Figs. 17c and 18c). This SLP development is accompanied by a rapid warm-up of the southwestern subtropical Indian Ocean. Together with the cold SST anomalies persistent in the eastern Indian Ocean from the previous season, the subtropical dipole SST pattern forms (Figs. 17b and 18d). The rapidly growing SLP and SST anomalies within a season imply intensive air–sea feedback, downstream from the northward expansion of the positive SLP anomalies in the previous season. The specific process needs further study using higher-frequency data.

By austral winter (JJA), the wind and SST anomalies mostly disappeared in the extratropical ocean (not shown). However, there are some lingering effects on the tropical Indian Ocean. Figure 18e shows the persistent cyclonic SLP center located at 20°S and 60°E, which extends both northwestward across the equator along the African coast and southeastward to the central subtropical ocean. Its core strength, however, has been reduced to less than 1 hPa from 3 hPa in the previous season. The warm SST anomalies are also persistent (Fig. 18f). Centered at 15°S and 60°E with a magnitude of 0.5°C, the SST anomalies are tilted in the same way as the SLP anomalies. Besides the effect of the surface heat fluxes, the anomalously warm surface center is influenced by the persistent HC anomalies located at nearly the same position.

Together with weaker cold SST anomalies centered near the same latitude farther east (around 100°E), these persistent SST anomalies maintain a weak zonal SST gradient in the tropical ocean from late austral fall (MAM) to early winter (JJA). Therefore, the subtropical mode sometimes contributes to the tropical mode during the "time window" for the external influence of the tropical zonal development (Annamalai et al. 2003), just as the tropical mode does the other way around to the subtropics in austral summer (Fig. 11c; see also, Xie et al. 2002). However, the process generating the zonal SST gradient shown in Fig. 18f is different from the one that generates the tropical mode discussed in section 5 in some aspects. For instance, the SST anomalies are not associated with an anticyclonic atmospheric low-level circulation over the southeastern ocean but with a weak cyclonic circulation in the southwest. In general, the lead–lag correlations between the PCs of these two modes (Figs. 9e and 17e) are not significant statistically. Therefore, the interference between the two modes only plays a minor role in their respective evolutions.

7. Summary

We have examined the interannual variability in the tropical Indian Ocean simulated by a coupled ocean–atmosphere GCM with active air–sea interaction over the global ocean and restricted within the Indian Ocean to the north of 30°S. In the latter case, the sources of the interannual anomalies associated with the air–sea interactions outside the Indian Ocean are eliminated. It is found that the major spatial patterns of the observed upper-ocean heat content and sea surface temperature anomalies can be reproduced realistically by both simulations, which suggests that these patterns are determined intrinsically within the Indian Ocean Basin. The interannual variability shows two intrinsic modes—one characterized by the coupled basinwide fluctuation of the tropical thermocline, zonal SST gradient, and wind anomalies over the equatorial and southern tropical ocean dominant in boreal fall to winter; the other by substantial subtropical SST anomalies featuring an east–west gradient strongest in austral fall.

The global coupled (or GLOBE) simulation reproduces the connection between the tropical thermocline variability in the Indian Ocean and the El Niño–Southern Oscillation in the tropical Pacific during boreal fall, even though the Pacific ENSO cycle in this simulation is weaker than the observed in amplitude. The major model weakness here is the early decay of the El Niño anomalies in the eastern Pacific during boreal fall to winter, which shortens its influence on the Indian Basin. Another shortcoming of the model simulation is the weak oceanic waves in the Indian Ocean within the equatorial waveguide due to weak equatorial zonal winds, which generates the symmetric SST patterns with respect to the equator from boreal summer to early fall in the observations (Huang and Kinter 2002; Rao and Behera 2005). The coupled model, however, captures the thermocline disturbances to the south of the equator more realistically.

In the absence of ENSO in the CLIM simulation, the tropical oscillation is stimulated by atmospheric internal variability centered in the northwestern tropical Pacific that disturbs the convection over the warm pool. The enhanced monsoon condition in the northwestern Pacific during boreal summer drives the anomalous Hadley cell that induces stronger subsidence and anticyclonic circulation near the surface over the southeastern Indian Ocean. This triggers the same air–sea feedback within the Indian Ocean as we have discussed in the GLOBE case. This model result confirms the finding by Kajikawa et al. (2003) using observational datasets, which connects the equatorial Indian Ocean variability with the variations in the South China Sea/Philippine Sea. Kajikawa et al. (2003) suggest that the direct thermal cell over the western Pacific is a precursor of an Indian Ocean dipole event. They also point out that, apart from the Hadley cell, the convection in

the western Pacific is influenced by ENSO through an anomalous Walker circulation. Our CLIM experiment further isolates the former from the latter. Our results are also largely consistent with Annamalai et al.'s (2003) finding that the Indian Ocean zonal mode can be triggered by the SST anomalies in the western Pacific during boreal spring and summer. These western Pacific SST anomalies are likely associated with the anomalous monsoon condition in the northwestern Pacific. Our results suggest that the anomalous monsoon condition can also be established in the western Pacific by atmospheric internal variability.

The subtropical SST fluctuation, on the other hand, is mainly a response to surface heat flux forcing associated with atmospheric disturbances from the southern extratropics during austral summer and fall. In the model, the initial external forcing generates active air–sea feedback and a rapid development of SST anomalies in the subtropical Indian Ocean during austral summer and fall. This subtropical SST dipole pattern is similar to the one identified by Behera and Yamagata (2001) from observations and also is generally consistent with the modeling study by Suzuki et al. (2004), both of which demonstrate the roles played by the wind-induced latent heat flux on evolution of the interannual Indian Ocean subtropical dipole event. On the other hand, the dipoles identified by Suzuki et al. (2004) show less equatorward expansion than our model events. Their SST anomalies also peak earlier in austral summer.

Analyzing observational datasets, Xie et al. (2002) suggested that the tropical Indian Ocean mode leads the subtropical fluctuations in the southern Indian Ocean. They speculate that the Sumatra SST variability may excite atmospheric waves that pass over the subtropical ocean and generate SST anomalies in local summer. In our simulations, the tropical mode produces SST anomalies in the subtropical ocean during austral summer (e.g., Fig. 11c) consistent with Xie et al.'s (2002) results. On the other hand, the subtropical SST anomalies can generate SST anomalies in the tropical ocean in boreal late spring and summer. However, the interference between these tropical and subtropical modes must be very weak because their lead–lag correlations are statistically insignificant either way. On the lowest order, they can be treated as independent between each other.

Acknowledgments. This study is supported by a joint grant from the National Science Foundation, the National Oceanic and Atmospheric Administration, and the National Aeronautics and Space Administration. We thank Dr. Jensen and three anonymous reviewers for providing many constructive suggestions. We thank Prof. P. S. Schopf for the development of the Poseidon ocean model, which is used as the oceanic component of the coupled model for this study. We also thank Prof. D. Straus and an anonymous reviewer within COLA for carefully reading an early version of the manuscript and providing many constructive suggestions for its revision.

REFERENCES

Annamalai, H., R. Murtugudde, J. Potemra, S. P. Xie, P. Liu, and B. Wang, 2003: Coupled dynamics over the Indian Ocean: Spring initiation of the zonal mode. *Deep-Sea Res. II,* **50,** 2305–2330.

——, S. P. Xie, J. P. McCreary, and R. Murtugudde, 2005: Impact of Indian Ocean sea surface temperature on developing El Niño. *J. Climate,* **18,** 302–319.

Baquero-Bernal, A., M. Latif, and S. Legutke, 2002: On dipolelike variability of sea surface temperature in the tropical Indian Ocean. *J. Climate,* **15,** 1358–1368.

Behera, S. K., and T. Yamagata, 2001: Subtropical SST dipole events in the southern Indian Ocean. *Geophys. Res. Lett.,* **28,** 327–330.

Chao, Y., and S. G. H. Philander, 1993: On the structure of the Southern Oscillation. *J. Climate,* **6,** 449–468.

Davey, M. K., and Coauthors, 2002: STOIC: A study of coupled model climatology and variability in tropical ocean regions. *Climate Dyn.,* **18,** 403–420.

Dommenget, D., and M. Latif, 2002: A cautionary note on the interpretation of EOFs. *J. Climate,* **15,** 216–225.

Godfrey, J. S., 1996: The effect of the Indonesian throughflow on ocean circulation and heat exchange with the atmosphere: A review. *J. Geophys. Res.,* **101,** 12 217–12 237.

Gong, D., and S. Wang, 1999: Definition of Antarctic Oscillation index. *Geophys. Res. Lett.,* **26,** 459–462.

Goswami, B. N., J. Shukla, E. K. Schneider, and Y. C. Sud, 1984: Study of the dynamics of the intertropical convergence zone with a symmetric version of the GLAS climate model. *J. Atmos. Sci.,* **41,** 5–19.

Hall, A., and M. Visbeck, 2002: Synchronous variability in the Southern Hemisphere atmosphere, sea ice, and ocean resulting from the annular mode. *J. Climate,* **15,** 3043–3057.

Hastenrath, S., 2002: Dipoles, temperature gradients, and tropical climate anomalies. *Bull. Amer. Meteor. Soc.,* **83,** 735–738.

Huang, B., 2004: Remotely forced variability in the tropical Atlantic Ocean. *Climate Dyn.,* **23,** 133–152.

——, and E. K. Schneider, 1995: The response of an ocean general circulation model to surface wind stress produced by an atmospheric general circulation model. *Mon. Wea. Rev.,* **123,** 3059–3085.

——, and J. L. Kinter III, 2002: The interannual variability in the tropical Indian Ocean. *J. Geophys. Res.,* **107,** 3199, doi:10:1029/2001JC001278.

——, and J. Shukla, 2007: Mechanisms for the interannual variability in the tropical Indian Ocean. Part I: The role of remote forcing from the tropical Pacific. *J. Climate,* **20,** 2917–2936.

——, P. S. Schopf, and Z. Pan, 2002: The ENSO effect on the tropical Atlantic variability: A regionally coupled model study. *Geophys. Res. Lett.,* **29,** 2039, doi:10.1029/2002GL014872.

——, ——, and J. Shukla, 2004: Intrinsic ocean–atmosphere variability of the tropical Atlantic Ocean. *J. Climate,* **17,** 2058–2077.

Kajikawa, Y., T. Yasunari, and R. Kawamura, 2003: The role of the local Hadley circulation over the western Pacific on the zonally asymmetric anomalies over the Indian Ocean. *J. Meteor. Soc. Japan,* **81,** 259–276.

Kalnay, E., and Coauthors, 1996: The NCEP/NCAR 40-Year Reanalysis Project. *Bull. Amer. Meteor. Soc.,* **77,** 437–471.

Kawamura, R., 1994: A rotated EOF analysis of global sea surface temperature variability with interannual and decadal scales. *J. Phys. Oceangr.,* **24,** 707–715.

Kirtman, B. P., and J. Shukla, 2000: Influence of the Indian summer monsoon on ENSO. *Quart. J. Roy. Meteor. Soc.,* **126,** 213–239.

Klein, S. A., B. J. Soden, and N.-C. Lau, 1999: Remote sea surface temperature variations during ENSO: Evidence for a tropical atmospheric bridge. *J. Climate,* **12,** 917–932.

Lanzante, J. R., 1996: Lag relationships involving tropical sea surface temperatures. *J. Climate,* **9,** 2568–2578.

Lau, N. C., and M. J. Nath, 2000: Impact of ENSO on the variability of the Asian–Australian monsoons as simulated in GCM experiments. *J. Climate,* **13,** 4287–4309.

——, and ——, 2003: Atmosphere–ocean variations in the Indo-Pacific sector during ENSO episodes. *J. Climate,* **16,** 3–20.

——, and ——, 2004: Coupled GCM simulation of atmosphere–ocean variability associated with zonally asymmetric SST changes in the tropical Indian Ocean. *J. Climate,* **17,** 245–265.

Li, T., B. Wang, C.-P. Chang, and Y. Zhang, 2003: A theory for the Indian Ocean dipole–zonal mode. *J. Atmos. Sci.,* **60,** 2119–2135.

Manganello, J. V., and B. Huang, 2006: The influence of the mean state on the annual cycle and ENSO variability: A sensitivity experiment of a coupled GCM. COLA Tech. Rep. 218, 60 pp.

Masson, S., P. Delecluse, J.-P. Boulanger, and C. Menkes, 2002: A model study of the seasonal variability and formation mechanisms of the barrier layer in the eastern equatorial Indian Ocean. *J. Geophys. Res.,* **107,** 8017, doi:10.1029/2001JC000832.

Mechoso, C. R., and Coauthors, 1995: The seasonal cycle over the tropical Pacific in coupled ocean–atmosphere general circulation models. *Mon. Wea. Rev.,* **123,** 2825–2838.

Mellor, G. L., and T. Yamada, 1982: Development of a turbulence closure model for geophysical fluid problems. *Rev. Geophys. Space Phys.,* **20,** 851–875.

Meyers, G., 1996: Variation of Indonesian throughflow and the El Niño-Southern Oscillation. *J. Geophys. Res.,* **101,** 12 225–12 263.

Moorthi, S., and M. J. Suarez, 1992: Relaxed Arakawa–Schubert: A parameterization of moist convection for general circulation models. *Mon. Wea. Rev.,* **120,** 978–1002.

Murakami, T., and J. Matsumoto, 1994: Summer monsoon over the Asian continent and western North Pacific. *J. Meteor. Soc. Japan,* **72,** 719–725.

Murtugudde, R., and A. Busalacchi, 1999: Interannual variability of the dynamics and thermodynamics of the tropical Indian Ocean. *J. Climate,* **12,** 2300–2326.

Niiler, P. P., and E. B. Kraus, 1977: One-dimensional models of the upper ocean. *Modelling and Prediction of the Upper Layers of the Ocean,* E. B. Kraus, Ed., Pergamon, 143–172.

NODC, 1999: *World Ocean Atlas 1998: CD-ROM documentation, version 1.0.* NODC Internal Rep. 15, NESDIS/NOAA, 16 pp.

North, G. R., T. L. Bell, and R. F. Cahalan, 1982: Sampling errors in the estimation of empirical orthogonal functions. *Mon. Wea. Rev.,* **110,** 699–706.

Pacanowski, R. C., and S. G. H. Philander, 1981: Parameterization of vertical mixing in numerical models of tropical oceans. *J. Phys. Oceanogr.,* **11,** 1443–1451.

Pan, Y.-H., and A. Oort, 1990: Correlation analyses between sea surface temperature anomalies in the eastern equatorial Pacific and the world ocean. *Climate Dyn.,* **4,** 191–205.

Rao, S. A., and S. K. Behera, 2005: Subsurface influence on SST in the tropical Indian Ocean: Structure and interannual variability. *Dyn. Atmos. Oceans,* **39,** 103–135.

Reynolds, R. W., and T. M. Smith, 1994: Improved global sea surface temperature analyses using optimum interpolation. *J. Climate,* **7,** 929–948.

Saji, N. H., B. N. Goswami, P. N. Vinayachandran, and T. Yamagata, 1999: A dipole mode in the tropical Indian Ocean. *Nature,* **401,** 360–363.

Schneider, E. K., B. P. Kirtman, Y. Fan, and Z. Zhu, 2001: Retrospective ENSO forecasts: The effect of ocean resolution. COLA Tech. Rep. 109, 27 pp.

Schopf, P. S., and A. Loughe, 1995: A reduced gravity isopycnal ocean model: Hindcasts of El Niño. *Mon. Wea. Rev.,* **123,** 2839–2863.

Shapiro, R., 1970: Smoothing, filtering and boundary effects. *Rev. Geophys. Space Phys.,* **8,** 359–387.

Suzuki, R., S. K. Behera, S. Iizuka, and T. Yamagata, 2004: Indian Ocean subtropical dipole simulated using a coupled general circulation model. *J. Geophys. Res.,* **109,** C09001, doi:10.1029/2003JC001974.

Thompson, D. W. J., and J. M. Wallace, 2000: Annular modes in the extratropical circulation. Part I: Month-to-month variability. *J. Climate,* **13,** 1000–1016.

Venzke, S., M. Latif, and A. Villwock, 2000: The coupled GCM ECHO-2. Part II: Indian Ocean response to ENSO. *J. Climate,* **13,** 1371–1383.

Wallace, J. M., E. M. Rasmusson, T. P. Mitchell, V. E. Kousky, E. S. Sarachik, and H. von Storch, 1998: On the structure and evolution of ENSO-related climate variability in the tropical Pacific: Lessons from TOGA. *J. Geophys. Res.,* **103,** 14 241–14 259.

Wang, B., R. Wu, and K.-M. Lau, 2001: Interannual variability of the Asian summer monsoon: Contrasts between the Indian and the western North Pacific–east Asian monsoons. *J. Climate,* **14,** 4073–4090.

Webster, P. J., A. M. Moore, J. P. Loschnigg, and R. R. Leben, 1999: Coupled ocean–atmosphere dynamics in the Indian Ocean during 1997–98. *Nature,* **401,** 356–360.

Xie, S.-P., H. Annamalai, F. A. Schott, and J. P. McCreary Jr., 2002: Structure and mechanisms of South Indian Ocean climate variability. *J. Climate,* **15,** 864–878.

Yamagata, T., S. K. Behera, J. J. Luo, S. Masson, M. R. Jury, and S. A. Rao, 2004: Coupled ocean-atmosphere variability in the tropical Indian Ocean. *Earth's Climate: The Ocean-Atmosphere Interaction, Geophys. Monogr.,* Vol. 147, Amer. Geophys. Union, 189–212.

Yu, J.-Y., and K. M. Lau, 2004: Contrasting Indian Ocean SST variability with and without ENSO influences: A coupled atmosphere-ocean GCM study. *Meteor. Atmos. Phys.,* **90,** 179–191.